RESEARCH ARTICLE

Key Points:
- Transient landscape response to base-level fall in the northeastern Tibetan Plateau
- Geomorphic features are consistent with measured erosion rates and estimated transport capacity
- Low rates of incision relative to sediment supply control lack of channel narrowing in this transient landscape

Correspondence to:
H. Zhang,
huiping@ies.ac.cn

Characterizing the transient geomorphic response to base-level fall in the northeastern Tibetan Plateau

Huiping Zhang[1] iD, Eric Kirby[2] iD, John Pitlick[3] iD, Robert S. Anderson[4] iD, and Peizhen Zhang[1,5]

[1]State Key Laboratory of Earthquake Dynamics, Institute of Geology, China Earthquake Administration, Beijing, China, [2]College of Earth, Ocean, and Atmospheric Sciences, Oregon State University, Corvallis, Oregon, USA, [3]Department of Geography, University of Colorado Boulder, Boulder, Colorado, USA, [4]Department of Geological Sciences and Institute of Arctic and Alpine Research, University of Colorado Boulder, Boulder, Colorado, USA, [5]School of Earth Science and Geological Engineering, Sun Yat-Sen University, Guangzhou, China

Abstract Analysis of hillslope gradient, landscape relief, and channel steepness in the Daxia River basin provides evidence of a transient geomorphic response to base-level fall on the northeastern Tibetan Plateau. Low-gradient channels and gentle hillslopes of the upper watershed are separated from a steeper, high-relief landscape by a series of convex knickzones along channel longitudinal profiles. Downstream projection of the "relict" portions of the profiles implies ~800–850 m of incision, consistent with geologic and geomorphic records of post ~1.7 Ma incision in the lower watershed. We combine optically stimulated luminescence dating of fluvial terrace deposits to constrain incision rates downstream of knickpoints with catchment-averaged ^{10}Be concentrations in modern sediment to estimate erosion rates in tributary basins both above and below knickpoints. Both sources of data imply landscape lowering rates of ~300 m Ma^{-1} below the knickpoint and ~50–100 m Ma^{-1} above. Field measurements of channel width ($n = 48$) and calculations of bankfull discharge ($n = 9$) allow determination of scaling relations among channel hydraulic geometry, discharge, and contributing area that we employ to estimate the patterns of basal shear stress, unit stream power, and bed load transport rate throughout the channel network. Our results imply a clear downstream increase of incision potential; this result would appear to be consistent with a detachment-limited response to imposed base-level fall, in which steepening of channels drives an increase in erosion rates. In contrast, however, we do not observe apparent narrowing of channels across the transition from slowly eroding to rapidly eroding portions of the watershed. Rather, the present-day channel morphology as well as its scaling of hydraulic geometry imply that the river is primarily adjusted to transport its sediment load and suggest that channel morphology may not always reflect the presence of knickpoints and differences in landscape relief.

1. Introduction

The past two decades have seen significant advances in our understanding of how landscape topography in active mountain ranges reflects the competition between climatically modulated erosion, lithologic erodibility, and tectonically driven uplift of rock [e.g., *Howard et al.*, 1994; *Whipple et al.*, 2000; *Montgomery and Brandon*, 2002; *Kirby and Whipple*, 2012]. Notably, much of this understanding relies on models of steady-state fluvial incision, where incision balances local rock uplift rate [*Howard*, 1994] such that the shape of equilibrium river channel profile remains steady through time [e.g., *Whipple and Tucker*, 1999]. These studies underscore that the steepness of the river profile, a measure of channel gradient normalized for differences in contributing drainage basin area [*Wobus et al.*, 2006b], directly influences landscape relief in active mountain ranges [*Whipple et al.*, 1999]. Although many formulations of channel incision into bedrock consider that incision rate is linearly dependent on channel gradient [e.g., *Howard et al.*, 1994; *Rosenbloom and Anderson*, 1994; *Whipple et al.*, 1999; *Whipple*, 2004], empirical studies from active mountain belts suggest that the relationship between channel steepness and erosion rate is nonlinear, implying that, as channel gradient increases, channels become more efficient at incising [e.g., *Snyder et al.*, 2000; *Duvall et al.*, 2004; *Ouimet et al.*, 2009; *DiBiase et al.*, 2010; *Kirby and Whipple*, 2012; *Harel et al.*, 2016]. This behavior likely reflects the combination of a threshold shear stress required for fluvial erosion [*Howard*, 1994; *Tucker*, 2004; *Lague et al.*, 2005] and a frequency-magnitude distribution of runoff [*Tucker and Bras*, 2000; *Molnar et al.*, 2006], such that steeper channels experience more frequent erosive discharge events [*Snyder et al.*, 2003a, 2003b; *DiBiase and*

Whipple, 2011; *Lague*, 2014]. Although hillslopes reach a threshold gradient at high erosion rate [*Schmidt and Montgomery*, 1995; *Burbank et al.*, 1996; *Heimsath et al.*, 2012], the apparent sensitivity of channel steepness to both incision thresholds and runoff variability [*Lague et al.*, 2005; *DiBiase and Whipple*, 2011] suggests that the limits to landscape relief in active mountain ranges may be more dependent on climate state and rock mass quality than previously inferred [e.g., *Whipple and Tucker*, 1999].

Similarly, important insights have been gained from the study of the transient response of landscapes to changes in relative base level, caused by either rock uplift or base-level fall. Implicit in these studies is the notion that the morphologic signature of a transient response can be recognized as a migrating boundary that marks the transition from one steady state to another [e.g., *Kirby and Whipple*, 2012; *Whittaker*, 2012]. During a transient response to either an increase in uplift rate or rate of base-level fall, steepening of the river profile generates convex portions of the river profile, or knickpoints [e.g., *Bishop et al.*, 2005], that separate upstream "relict" reaches of the fluvial system that have not yet adjusted to the new boundary condition from downstream reaches which have begun to adjust [*Schoenbohm et al.*, 2004; *Crosby and Whipple*, 2006; *Berlin and Anderson*, 2007; *Harkins et al.*, 2007; *Whittaker et al.*, 2007b]. A family of river incision models that considers channel incision rate to scale with boundary shear stress and/or unit stream power ("detachment-limited" models) [e.g., *Howard et al.*, 1994; *Whipple and Tucker*, 1999; *Whipple*, 2004; *Attal et al.*, 2011] yields transient river profiles characterized by knickpoints [e.g., *Whipple and Tucker*, 1999] that migrate through the channel network as kinematic waves [e.g., *Rosenbloom and Anderson*, 1994; *Whipple*, 2004]. However, as sediment supply approaches or exceeds transport capacity, channel gradients will dynamically adjust to achieve equilibrium transport of sediment [*Tucker and Whipple*, 2002]. In these "transport-limited" systems, the response to a change in boundary conditions migrates as a diffusive wave of gradient adjustment and river profiles are not expected to develop discrete convexities [*Whipple and Tucker*, 2002; *Tucker*, 2004; *Whipple*, 2004]. Attempts to discriminate between these end-members in natural field settings have met mixed success; some studies conclude that a detachment-limited model adequately describes the system behavior [*Attal et al.*, 2008, 2011; *Whittaker et al.*, 2007b, 2008], while others suggest that a transport-limited model is required [*Cowie et al.*, 2008; *Valla et al.*, 2010; *Whipple and Tucker*, 2002], and yet others argue that neither of these two end-members are sufficient [*Tomkin et al.*, 2003; *van der Beek and Bishop*, 2003].

Central to any model of fluvial response to a change in boundary conditions is whether or not the hydraulic geometry of the channel dynamically adjusts to increase boundary shear stress along the bed and banks [*Parker*, 1979]. Although most models of bedrock channel incision presume that channel width (W) follows a power law scaling with discharge (Q) or drainage area (A, a proxy for Q), similar to that observed in alluvial channels ($W \propto Q^{0.5}$) [*Hack*, 1957; *Wohl and David*, 2008], field studies of natural channels present conflicting observations. Measurements of channel width in some fluvial systems with both alluvial and bedrock reaches exhibit similar scaling [*Montgomery and Gran*, 2001; *Whipple*, 2004; *Whitbread et al.*, 2015], even in regions with strongly varying rock uplift rate [*Snyder et al.*, 2003a], suggesting that channel width is governed by a similar set of processes in both mobile and fixed substrates. In contrast, several recent field studies document systematic variations in channel width in channels adjusted to varying rates of base-level fall or rock uplift [*Duvall et al.*, 2004; *Finnegan et al.*, 2005; *Amos and Burbank*, 2007; *Yanites et al.*, 2010; *Kirby and Ouimet*, 2011]. Moreover, channel narrowing appears to be a primary means by which rapidly incising fluvial systems initially respond to base-level fall [*Amos and Burbank*, 2007; *Whittaker et al.*, 2007a, 2007b, 2008], a response that may be amplified by variations in rock erodibility [*Attal et al.*, 2011; *Fisher et al.*, 2012, 2013; *Allen et al.*, 2013]. Although the process of width adjustment remains incompletely understood, recent models that explicitly consider channel cross-sectional geometry [e.g., *Stark*, 2006; *Wobus et al.*, 2006a; *Turowski et al.*, 2007; *Yanites and Tucker*, 2010] suggest that spatially variable bedrock wear associated with the degree of sediment cover on the bed [e.g., *Sklar and Dietrich*, 2004] is a primary determining factor.

Recently, channel incision models have been utilized to formally invert river profile morphology for uplift histories [e.g., *Pritchard et al.*, 2009; *Roberts and White*, 2010; *Roberts et al.*, 2012; *Goren et al.*, 2014; *Stephenson et al.*, 2014; *Wilson et al.*, 2014; *Fox et al.*, 2014, 2015; *Glotzbach*, 2015; *Rudge et al.*, 2015]. Despite the quantitative appeal of such models, application to natural systems requires a set of assumptions regarding the manner in which channels adjust to differential uplift of rock; primary among these is the requirement that channel gradients adjust linearly to changes in incision and/or uplift rate.
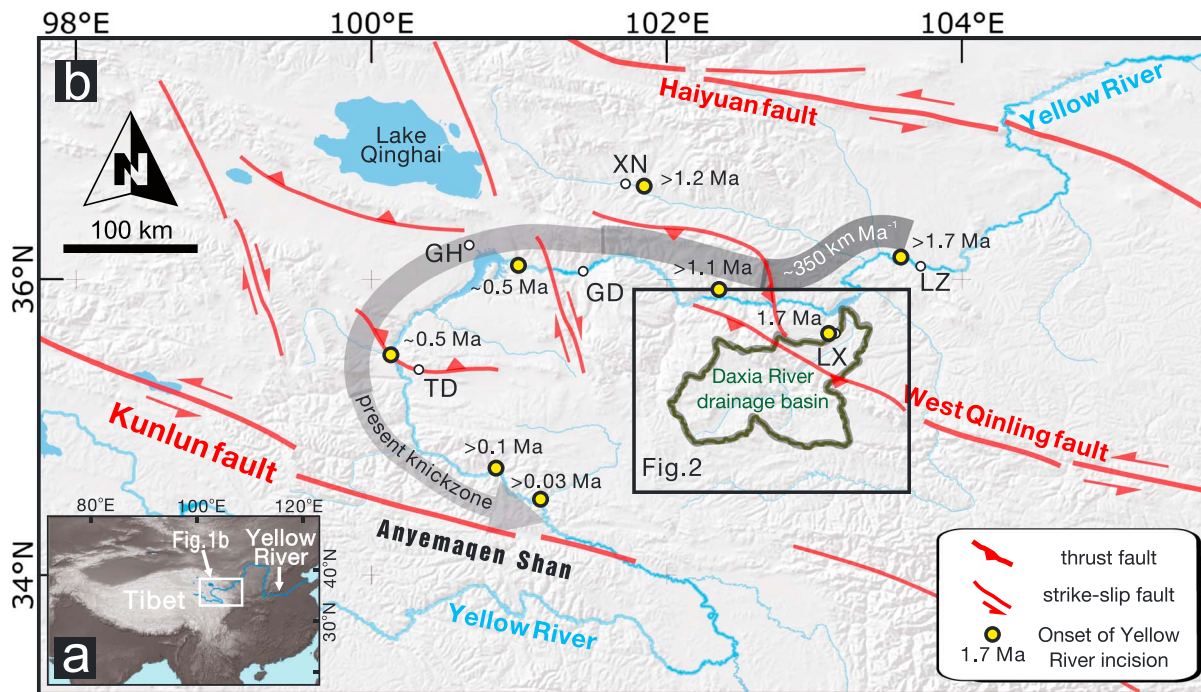
Figure 1. Geomorphic setting of the (a) Yellow River and the (b) Daxia River basin in northeastern Tibetan Plateau. Along the Yellow River, an incision wave propagated quickly through the Lanzhou (LZ), Linxia (LX), Xining (XN), Guide (GD), Gonghe (GH), and Tongde (TD) basins into the inner plateau at ~350 km Ma^{-1} and left a transient knickzone to the north of the Kunlun fault [*Craddock et al.*, 2010; *Harkins et al.*, 2007; *Zhang et al.*, 2014]. Initiation of incision in the Linxia (LX) basin is estimated to have begun at ~1.7 Ma.

The wide range in the behavior of fluvial systems subjected to base-level fall highlights the limits of our understanding and suggests a need for additional data from field sites where boundary conditions are reasonably well known. In this manuscript, we exploit such a setting in the northeastern Tibetan Plateau, where drainage basin integration along the Yellow River during the Pleistocene [*Craddock et al.*, 2010] engendered a wave of rapid incision along the Yellow River that propagated into the plateau interior (Figure 1) [*Harkins et al.*, 2007; *Craddock et al.*, 2010; *Zhang et al.*, 2014]. This incision induced a sudden base-level fall along tributaries of the Yellow River to which the landscape has not yet completely adjusted. We focus on one of these tributaries, the Daxia River, which drains the margin of the Tibetan Plateau across the Linxia basin (Figure 1). Preserved remnants of low-relief topography previously interpreted as a relict erosional surface exist in the headwater regions of the catchment [*Clark et al.*, 2010], and these surface remnants are separated from a downstream region of high relief and high incision rates [e.g., *Li et al.*, 1997] by a series of knickpoints along the channel network. We combine measurements of average erosion rate from ^{10}Be concentrations in modern sediment, optically stimulated luminescence (OSL) dating of fluvial strath terraces and analyses of river profiles to quantify the rate of landscape lowering across this transition and to characterize the morphologic adjustment of the channel profile to base-level fall. To evaluate the role of changes in channel width during transient incision, we made detailed field measurements of channel geometry, slope, and grain size at a series of reaches along the system. We assess whether these observations reflect a response of the Daxia River to imposed base-level fall along the Yellow River that is characteristic of detachment-limited or transport-limited systems. Finally, we explore the implications of the results of this analysis for the response time of the landscape and for the interpretation of transient fluvial systems in general.

2. Background: Pleistocene Incision Along the Daxia River

Deep canyons carved into the northeastern Tibetan Plateau along the Yellow River and its tributaries attest to rapid incision in the Quaternary [*Li*, 1991; *Li et al.*, 1997]. Although these early workers attributed incision to rapid uplift of the Tibetan Plateau, a large body of geologic studies now demonstrates that significant crustal thickening and basin development took place during the latter part of the Miocene [*Craddock et al.*, 2011;

Fang et al., 2003; *Hough et al.*, 2011; *Lease et al.*, 2007, 2012; *Yuan et al.*, 2013; *Zhang et al.*, 2012]. Moreover, incision along the Yellow River initiated near the plateau margin at ~1.8 Ma and progressed systematically upstream at average rates of ~350 km Ma^{-1} [*Craddock et al.*, 2010]. Although flexural isostatic response to unloading associated with rapid incision may have facilitated the Pleistocene reorganization of a portion of the river network [*Zhang et al.*, 2014], the present location of the incisional wave is marked by a series of transient knickzones throughout the Yellow River watershed north of the Kunlun fault, within the Anyemaqen Shan (Figure 1) [*Harkins et al.*, 2007].

Our field site is located along the Daxia River, a tributary to the Yellow River that flows across the northeastern margin of the Tibetan Plateau (Figure 1). With three tributary channels of comparable dimension (labeled North (NF), West (WF), and East (EF) Forks on Figure 2a), the ~200 km long Daxia River originates in bedrock units of the West Qinling range (Figure 2), including Late Triassic-Jurassic granites and granodiorites that intrude low-grade, deformed Paleozoic and Triassic age metasedimentary rocks (Figure 2a) [*Bureau of Geology and Mineral Resources (BGMR) Gansu Province*, 1989]. These rocks are separated from Cretaceous-Pliocene terrestrial conglomerates, sandstones, and mudstones in the Linxia basin [e.g., *Fang et al.*, 2003] by the West Qinling fault to the north (Figure 2a). Subsidence patterns in the Linxia basin derived from several measured stratigraphic sections [*Fang et al.*, 2003] are interpreted to reflect basin formation in response to flexural loading along its southern margin by slip on the West Qinling fault, consistent with cooling histories from the footwall of this fault system [*Clark et al.*, 2010] and from dating of fault gouge [*Duvall et al.*, 2011]. However, the absence of fault scarps and displaced landforms suggest that, if the fault is active at present, then activity is limited to a blind tip beneath the basin (Figures 1 and 2).

The Daxia River drainage basin has an area of ~7200 km^2 (Figure 2b) and a mean elevation of ~3200 m; total relief from the headwater divide to the confluence with the Yellow River is ~2800 m. The headwater regions between 3200 and 3800 m elevation are characterized by gentle topographic gradients (slope < 10°) and low relief (Figure 3). East and west of the canyon of the Daxia River, these regions of low slope have been interpreted as remnants of a paleoerosional landscape [*Clark et al.*, 2010]. Meter-thick soils typically mantle the bedrock across the low-relief surface (Figures 4a and 4b). Downstream, however, strath terraces are developed within the canyons along forks of the Daxia River (Figure 4c) and hillslopes bounding the canyon walls increase to 30–40° (Figure 3). Consistent with the slope distribution in the basin (Figure 3a), the local relief (defined as the difference in elevations measured within a 1 km^2 window) also increases downstream, reaching ~500 m immediately south of the West Qinling fault (Figure 3b). In the Linxia basin, north of the West Qinling fault, however, slope and local relief decrease abruptly to <20° and <200 m, respectively (Figure 3).

These geomorphic characteristics appear to reflect recent incision along the Daxia River in response to down-cutting of the Yellow River trunk stream during drainage basin integration in the early Pleistocene [*Craddock et al.*, 2010]. Magnetostratigraphic studies of terrestrial basin fill in the Linxia basin constrain the initiation of incision at ~1.8 Ma (Figures 1 and 2) [*Li et al.*, 1997; *Fang et al.*, 2003]. Subsequent downcutting generated at least seven levels of terraces along the Daxia River in the Linxia basin [*Li et al.*, 1997; *Fang et al.*, 2003] near Linxia city (LX in Figure 1). Magnetostratigraphic dating of paleosol-loess sequences developed atop the highest terrace, ~500 m above the present Daxia River, suggests terrace abandonment at ~1.7 Ma [*Li et al.*, 1997; *Fang et al.*, 2003]. Thus, the onset of incision is tightly bound between ~1.8 Ma and ~1.7 Ma. Average rates of downcutting since that time appear to have been ~300 m Ma^{-1}, but the separation between terrace treads suggests that incision rates in the interval between ~1.7 Ma and ~1.4 Ma may have approached ~1 km Ma^{-1} during the initial phase of response to base-level fall [*Li et al.*, 1997].

3. Methods

We have taken multiple approaches to quantify the transient response of the Daxia River. First, we surveyed channel geometry, grain size, and reach-averaged gradient at selected sites along river reaches where human disturbance to channels was limited (Figures 2 and 4), ensuring to conduct surveys above and below knickpoints. Second, to quantify the erosion rates both upstream and downstream of knickpoints, we sampled active channel sands from tributary catchments for ^{10}Be measurements (Figure 2b) [e.g., *Granger et al.*, 1996]. To facilitate a comparison with existing measurements from eastern Tibet [e.g., *Harkins et al.*, 2007; *Ouimet et al.*, 2009; *Kirby and Harkins*, 2013], and to minimize the potential influence of landslides on
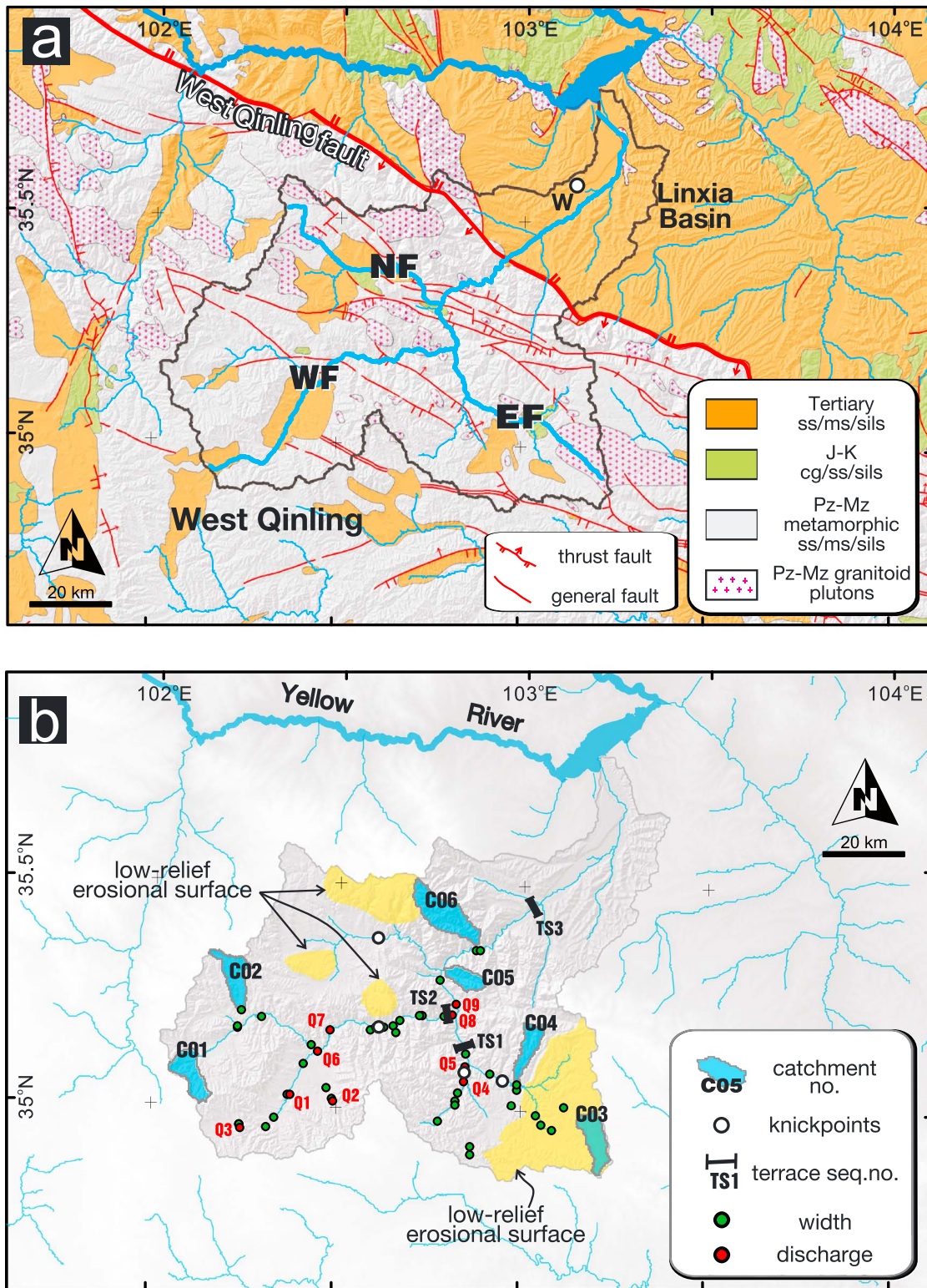
Figure 2. (a) Geological and (b) geomorphic features of the Daxia River catchment. Abbreviations of cg/ss/ms/sils mean conglomerates, sandstone, mudstone, and siltstone, respectively. The black line is the outline of the Daxia River basin. NF, WF, and EF are North Fork, West Fork, and East Fork of the Daxia drainage; W is the Wangjiashan site to constrain initiation of river incision at 1.7 Ma [*Li et al.*, 1997] (Figure 2a). The green and red dots in Figure 2b are our field sites for channel width (no. = 48) and discharge (no. = 9) (Q1–Q9) measurements, respectively. The light blue polygons with numbers (C01–C06) are subcatchments for ^{10}Be catchment erosion rates. TS1-3 are strath terrace series sampled for OSL dating to infer incision rates. The white dots with black outline are major knickpoints. Low-relief erosional surfaces in yellow are modified from *Clark et al.* [2010].
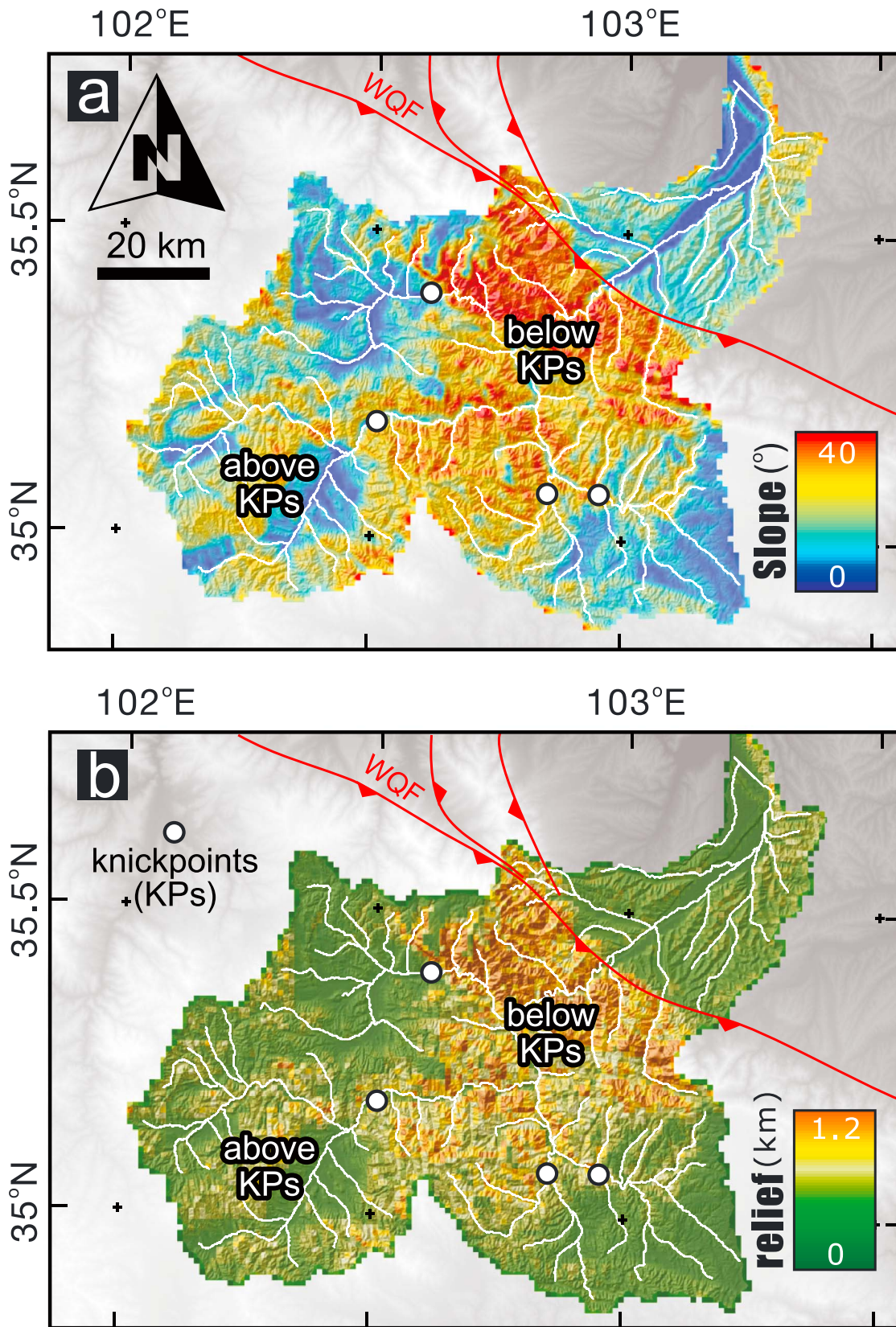
Figure 3. (a) Slope and (b) local relief (1 km × 1 km window) showing the distribution of the transient landscape features of the Daxia catchment. Note the obvious difference in slope and relief upstream and downstream of the knickpoints.
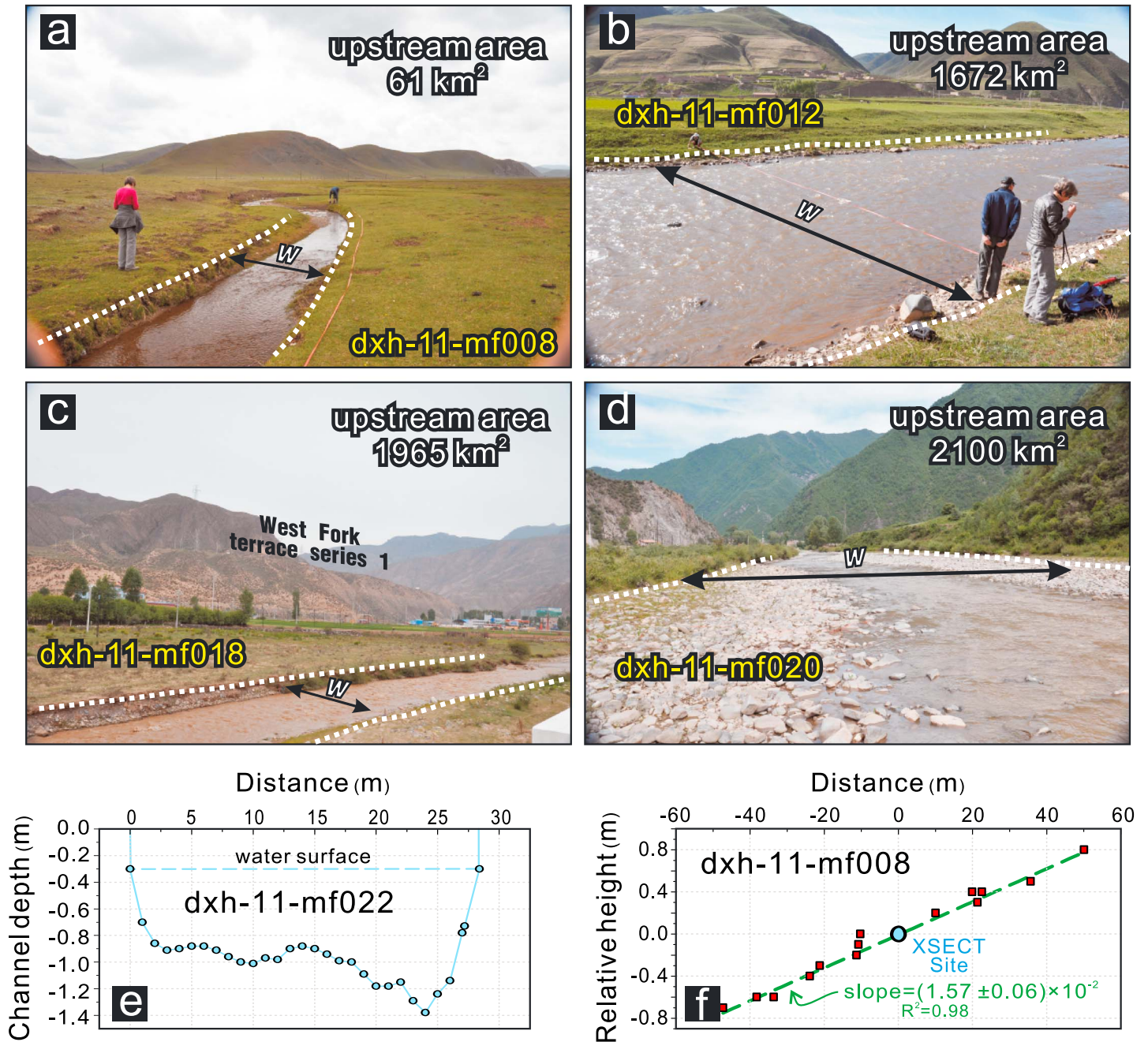
Figure 4. (a–d) Field photos showing the sites for discharge and channel width surveys. Note the downstream (Figures 4a–4d) increasing relief of the landscape; Figures 4a and 4b are taken above knickpoints, and Figures 4c and 4d are from channels downstream of the knickpoints. Shown also are the upstream drainage basin dimensions and bankfull channel boundaries for width (*W*) measurement at each cross-section. (e) Sample cross-section survey at dxh-11-mf022 site (Table 1 for location); each point (~1 m apart) represents a depth survey point across the section. (f) Reach-scale channel gradient determined at site dxh-11-mf008. A laser rangefinder (precision ~1 cm) and a surveying rod were used to document the relative height of water surface both ~50 m downstream and upstream of the cross-section (XSECT) site.

cosmogenic inventories [e.g., *Niemi et al.*, 2005; *Yanites et al.*, 2009], we sampled catchments with drainage areas of ~40–100 km^2. Third, in an effort to further characterize the rate of channel incision downstream of knickpoints, we determined incision rates by dating strath terraces (Figure 2b). We mapped and surveyed the height of strath terraces, and we collected and analyzed samples of medium sand from selected terrace treads for optically stimulated luminescence (OSL) dating; reach-scale incision rates were calculated from the

Table 1. ^{10}Be Catchment Erosion Rates and Catchment Geometrics (Uncertainties Are All Given in 2σ)

Sample No.	Lat. (°N)	Lon. (°E)	Drainage Area (km^2)	Mean Elev. (m)	Average Production Rate (at. g$_{qtz}$$^{-1}$ yr^{-1})	Shielding Factors	^{10}Be Concentration (10^6 at. g$_{qtz}$$^{-1}$)	^{10}Be Erosion Rate (m Ma^{-1})	k_{sn} (m$^{0.9}$)	Relief (m)	Mean Slope (deg)
C01	35.07	102.99	66.22	3761	53.99	0.999	6.48 ± 0.63	114.9 ± 20.4	55.8 ± 1.0	175.5 ± 48.8	12.6 ± 3.3
C02	35.12	102.13	65.10	3609	61.12	0.999	22.49 ± 0.65	79.6 ± 9.3	63.6 ± 5.3	164.4 ± 45.5	11.6 ± 2.6
C03	35.00	103.15	65.34	3511	53.00	1.000	26.67 ± 3.60	34.1 ± 13.1	40.2 ± 5.9	57.1 ± 18.5	4.3 ± 1.4
C04	35.22	102.24	47.89	3523	56.58	0.998	57.16 ± 0.18	145.1 ± 13.1	109.3 ± 4.9	232.0 ± 81.0	15.9 ± 3.9
C05	35.31	102.79	39.11	3068	41.89	0.995	4.17 ± 0.36	322.6 ± 32.0	203.2 ± 9.9	369.8 ± 91.7	20.5 ± 4.0
C06	35.40	102.87	108.95	3377	51.40	0.992	6.90 ± 0.45	334.2 ± 28.5	188.6 ± 16.6	424.8 ± 95.5	25.2 ± 4.0

height of the terrace and present-day river level. Fourth, we analyzed stream profiles from a 90 m resolution Shuttle Radar Topography Mission digital elevation model (SRTM-DEM) and identified knickpoints by following the methods of *Kirby et al.* [2003] and *Kirby and Whipple* [2012] to characterize the shape of river profiles across the boundary between the incised and unincised portions of the watershed. We projected relict profiles by using data from channel segments above the knickpoints to estimate the amount of incision along downstream reaches [*Kirby and Whipple*, 2012; *Miller et al.*, 2013]. Fifth, based on the field measurements of channel width, depth, grain size, and local channel slope (Figure 4), we determined the incision potential by calculating the unit stream power and boundary shear stress and bed load transport capacity at bankfull flow. Following available formulations, we then modeled a distribution of unit stream power and basal shear stress within the Daxia catchment. Finally, we assembled the analyses of stream profiles, measurements of channel geometry, calculations of stream power/shear stress, and estimates of the rates of catchment erosion and reach-scale incision to develop a quantitative picture of the transient geomorphic response of the Daxia River to Yellow River incision.

3.1. ^{10}Be Basin-Averaged Erosion Rates

Concentrations of cosmogenic radionuclide ^{10}Be can be interpreted in terms of drainage-basin average erosion rates [e.g., *Granger et al.*, 1996, 2013; *Bierman and Steig*, 1996]. In a steadily eroding landscape with rock density ρ_r (=2.7 g/cm^3), the catchment-averaged erosion rate (ε) will be

$$\varepsilon = \frac{P_{avg}\Lambda}{N\rho_r} \tag{1}$$

where N is the ^{10}Be concentration in sediment, P_{avg} is the average production rate within the catchment, and Λ is the production attenuation scale in rock (~160 g cm^{-2}) [*Lal*, 1991]. Solving equation (1) for ε requires estimates of P_{avg}. Using the Microsoft Excel calculator Cosmocalc [*Vermeesch*, 2007], we scaled the cosmogenic nuclide production rates for each pixel (~90 m × ~90 m) from SRTM-DEM data for both elevation and latitude to obtain the catchment-averaged production rate [*Lal*, 1991; *Stone*, 2000]. Corrections were neglected for quartz enrichment, magnetic field variations, or snow/ice cover, simplifications that are justified by the fact that the Daxia River drainage basin features relatively uniform lithology and that snow fall is rare in this arid catchment that has not been intensively glaciated. We report the shielding factor related to catchment topography, calculated with the algorithm of *Codilean* [2006] by using a 90 m resolution SRTM-DEM (Table 1).

To compare the erosion rates across the transient landscape, samples were collected above the tributary junction for ~50–100 km^2 catchments upstream and downstream of knickpoints (Table 1 and Figure 2). As each catchment is underlain by a single dominant lithology (Figure 2a), we assume a uniform quartz distribution. To avoid the effects of long-term sediment storage on ^{10}Be concentration, samples were typically taken away from the floodplains and terraces. In total, four samples were collected from catchments upstream of the knickpoints and two samples downstream of the knickpoints to avoid the need to deconvolve signals from relict and adjusted topography. To measure ^{10}Be concentrations of the sediments, we first physically and chemically isolated quartz from our samples, following a standard protocol at the University of Colorado Boulder [*Yuan et al.*, 2011; *Zhang et al.*, 2014]. The ^{10}Be concentrations were then measured by accelerator mass spectrometry at the Purdue Rare Isotope Measurement Laboratory accelerator mass spectrometry facility (Table 1).

Table 2. OSL Dating and Incision Rates From Strath Terraces (Uncertainties Are All Given in 2σ)

Sample No.	Depth (m)	Bulk Alpha ($ks^{-1} cm^{-2}$)	K_2O (%)	Water Content (%)	Dose Rate ($Gy\ ka^{-1}$)	Equivalent Dose (Gy)	OSL Age (ka)	Terrace Height (m)	Incision Rate ($m\ Ma^{-1}$)
DXH-O-01 (TS1)	0.5	9.76 ± 0.32	1.71	1	3.49 ± 0.20	187.0 ± 4.8	53.6 ± 1.6	13.1 ± 0.2	244.4 ± 8.2
DXH-O-02 (TS1)	0.5	10.82 ± 0.31	1.8	1	3.76 ± 0.21	201.2 ± 8.1	53.5 ± 2.3	28.5 ± 0.5	532.7 ± 24.7
DXH-O-03 (TS2)	0.5	10.54 ± 0.30	1.78	1	3.73 ± 0.20	161.4 ± 2.1	43.2 ± 0.9	14.3 ± 0.2	331.0 ± 8.3
DXH-O-04 (TS2)	2.5	10.29 ± 0.31	1.76	2	3.61 ± 0.20	215.7 ± 5.5	59.8 ± 1.7	45.4 ± 0.8	759.2 ± 25.4
DXH-O-07 (TS3)	2.7	8.90 ± 0.25	1.56	8	3.55 ± 0.20	30.1 ± 0.6	10.4 ± 0.4	12.7 ± 0.2	1221.2 ± 50.8

3.2. Strath Terrace Chronology

For further comparison with the catchment-averaged erosion rates, we also mapped and sampled several flights of strath terraces (TS1 and TS2) downstream of the knickpoints (Figure 2b). One individual strath terrace (TS3) was also sampled within the Linxia basin (Figure 2b). Heights of strath terrace (the contact between overlying channel sediments and bedrock) above the present active channel were measured with a TruPulse 200 laser rangefinder (nominal precision to ~1 cm). To obtain a reliable chronology for the terrace sequence, optically stimulated luminescence (OSL) dating was carried out (Table 2). OSL samples were collected from loess and sand ~20 cm above the gravel on the terraces for all the terraces to constrain the minimum ages of the terrace treads. After removing at least 10 cm (usually much more) of the face of the outcrop, samples were collected by using ~20 cm × 5 cm metal cylinders and capped by silver paper and tape to prevent further exposure. Sample pretreatment and preparation were carried out, following a standard protocol at the State Key Laboratory of Earthquake Dynamics, Institute of Geology, China Earthquake Administration [*Yuan et al.*, 2011].

3.3. Stream Profile Analysis

The interpretation of river profiles in actively incising mountain belts relies on the notion that, in regions of uniform rock strength, runoff, and rock uplift rate, steeper channels should be associated with higher rates of incision and therefore uplift at steady state [*Snyder et al.*, 2000; *Duvall et al.*, 2004; *Kirby and Whipple*, 2012; *Wobus et al.*, 2006b]. It has long been recognized that rivers exhibit an empirical scaling between local channel slope (*S*) and the contributing drainage area upstream (*A*), such that a river profile can be described in terms of steepness (k_s) and concavity (θ) indices [*Hack*, 1957; *Flint*, 1974]:

$$S = k_s A^{-\theta} \tag{2}$$

To compare channel steepness among different channel segments, one must account for correlations between the steepness index and concavity index [e.g., *Kirby et al.*, 2003; *Wobus et al.*, 2006b]. We calculate the channel slope over 1 km reaches, employ a fixed reference concavity index ($\theta_{ref} = 0.45$, equation (3)), and report the normalized steepness index (k_{sn}) [*Snyder et al.*, 2000; *Kirby and Whipple*, 2001; *Kirby et al.*, 2003; *Duvall et al.*, 2004].

$$k_{sn} = SA^{\theta_{ref}} \tag{3}$$

The boundary-separating reaches with low channel steepness upstream from steeper reaches downstream can be readily identified on longitudinal profiles as an abrupt downstream increase in the scaling of channel gradient with contributing drainage area (see *Wobus et al.* [2006b] for a thorough explanation of this method). Such features can also be characterized by the scaling of a parameter chi (χ) with elevation in the catchment [*Harkins et al.*, 2007; *Royden and Taylor Perron*, 2013]. Chi (χ) represents the integral of basin area (*A*) evaluated with streamwise distance (*x*) as

$$\chi = \int_{x_b}^{x} \left(\frac{A_0}{A(x)} \right)^{\theta_{ref}} dx \tag{4}$$

where x_b is the position at the river mouth and A_0 is a reference drainage area; when A_0 is set to 1 km^2 and θ_{ref} to the same value as used in equation (3), the slope of the chi-elevation plot is equivalent to the normalized steepness index [*Royden and Taylor Perron*, 2013]. Thus, knickpoints that bound regions with varying channel steepness (k_{sn}) can be recognized as changes in slope on the chi-elevation plot.

We estimated the total incision by projecting the upstream relict channel profile, as in previous work [*Kirby and Whipple*, 2012; *Miller et al.*, 2013]. The longitudinal profiles of all the three forks of the Daxia River

(Figure 2a) were extrapolated by using the k_{sn} above the knickpoint and $\theta_{ref} = 0.45$. By applying k_{sn} and θ_{ref} for each channel segment, we solved equation (3) for local slope and extrapolated the profile downstream to the Yellow River. To estimate the amount of lowering of the "relict" profile upstream of the knickpoint, we exploit the known timing of the initiation of incision at ~1.7 Ma [*Li et al.*, 1997] and extrapolate the measured erosion rates back in time.

3.4. Field Surveys of Channel Geometry

In order to evaluate spatial patterns of incision potential, we surveyed a series of channel reaches and used measurements from these reaches to develop scaling relations between channel width, discharge, and drainage area. Although locally variable, channel width (W) and discharge (Q) for mountain rivers have been found to vary systematically with drainage area (A) in a manner similar to that observed in lowland alluvial channels, resulting in the widespread adoption of the following equations in landscape evolution models [*Hack*, 1957; *Snyder et al.*, 2000; *Montgomery and Gran*, 2001; *Wohl and David*, 2008]:

$$W = k_w A^a \tag{5}$$

$$Q = k_q A^b \tag{6}$$

where k_w and k_q are empirical coefficients and a and b are scaling exponents. Typically, the value of a ranges from 0.3 to 0.5 and the value of b ranges from 0.7 to 0.9 [*Snyder et al.*, 2000]. We combined digitally derived estimates of upstream drainage area with field measurements of channel properties to establish the relations given by equations (5) and (6). We measured the width of the active channel at 48 locations (Figure 2b and Tables 3 and 4). Active channel width was defined in the field by the break in slope between the floodplain and the channel and an absence of vegetation (considered equivalent to "bankfull width" in alluvial rivers). Wherever possible, ~10 measurements of width along a 150–200 m channel reach were taken at each survey site to account for reach-scale variations, which were then averaged to obtain a mean channel width (Table 3). We selected sites with relatively uniform channel morphology and sampled a broad range of drainage areas that spanned locations above and below major knickpoints. We avoided taking measurements in reaches that were heavily modified by human activities.

Additional measurements were taken at nine of these sites to estimate the bankfull discharge (Figure 2b), as well as the flow properties needed to calculate bed load transport capacity (Table 4). These sites were located within self-formed channel reaches where the bed and bank materials consisted of alluvium transported by the river. Bankfull discharge was estimated from the continuity equation,

$$Q = \overline{U}HW \tag{7}$$

where W is the bankfull channel width, H is the bankfull channel depth, and $\overline{U}$ is the bankfull velocity. A single cross section was surveyed at each reach site. Bankfull width and depth were determined from cross-section surveys (e.g., Figure 3e). Mean velocity, $\overline{U}$, was calculated from a flow resistance relation developed by *Keulegan* [1938], which can be written as

$$\overline{U} = 2.5\sqrt{gHS}\ln\left(\frac{11H}{3D_{84}}\right) \tag{8}$$

Here H is the bankfull channel depth, S is the local channel gradient, g is the acceleration due to gravity (9.8 m s^{-2}), and D_{84} represents the particle size for which 84% of particles are finer (Table 4). We measured channel geometry (H, W, and S) with a laser rangefinder, tape, and surveying rod (Figure 3). Channel gradients were determined by measuring changes in water-surface elevation along the edge of the channel over a distance of ~100 m. To determine the grain-size distribution of the channel bed material, we selected ~100 individual particles at random in the river bed over the entire extent of the study reach [*Wolman*, 1954] and determined the size of each particle by using a gravelometer (i.e., a metal template with graduated openings equivalent to 1/2 ψ sieve sizes ($\psi = \log D / \log 2$)).

3.5. Calculation of Bed Load Transport Capacity, Unit Stream Power, and Shear Stress

We used data from the nine field sites discussed in the previous section to derive site-specific (local) estimates of bed load transport capacity. Transport capacities were calculated for bankfull flow by using field data as input to a bed load transport function developed by *Parker* [1979]. This function can be written as

Table 3. Measurements of the Daxia River Channel Widths (W) and Drainage Basin Areas (A)

No.	Field Number	Latitude (deg)	Longitude (deg)	Elevation (m)	Width (m)	Drainage Area (km^2)
1	dxh-11-mf002	34.967	102.243	3430	7.6 ± 0.8	125.1
2	dxh-11-mf00201	34.967	102.243	3430	2.0 ± 0.2	21.5
3	dxh-11-mf003	34.962	102.315	3309	8.7 ± 0.7	162.7
4	dxh-11-mf004	34.984	102.338	3266	9.1 ± 1.2	241.0
5	dxh-11-mf005	35.035	102.369	3170	9.0 ± 0.7	362.0
6	dxh-11-mf007	35.106	102.411	3068	8.0 ± 0.3	556.0
7	dxh-11-mf009	35.029	102.491	3286	1.4 ± 0.3	14.3
8	dxh-11-mf010	35.055	102.473	3233	5.0 ± 0.8	86.6
9	dxh-11-wf001	35.209	102.296	3203	19.3 ± 1.9	639.5
10	dxh-11-wf002	35.221	102.239	3297	5.3 ± 0.5	61.1
11	dxh-11-wf003	35.183	102.230	3319	16.4 ± 0.8	316.3
12	dxh-11-wf004	35.184	102.232	3320	9.3 ± 0.6	132.3
13	dxh-11-wf005	35.148	102.430	3033	18.8 ± 0.8	825.4
14	dxh-11-mf013	35.186	102.591	2890	2.9 ± 0.2	31.8
15	dxh-11-mf014	35.190	102.604	2860	31.6 ± 3.1	1870.8
16	dxh-11-mf015	35.192	102.625	2878	32.2 ± 4.7	1890.3
17	dxh-11-mf016	35.195	102.652	2795	20.2 ± 3.5	1912.0
18	dxh-11-mf017	35.181	102.660	2834	4.9 ± 0.8	43.1
19	dxh-11-mf018	35.206	102.671	2760	22.0 ± 1.2	1965.2
20	dxh-11-mf019	35.219	102.725	2685	14.6 ± 1.8	2052.6
21	dxh-11-mf020	35.217	102.791	2564	23.0 ± 3.7	2100.0
22	dxh-11-ef001	34.969	103.085	3178	3.0 ± 0.2	85.2
23	dxh-11-ef002	34.980	103.056	3136	5.5 ± 0.3	119.9
24	dxh-11-ef003	35.021	103.117	3308	8.5 ± 1.2	108.9
25	dxh-11-ef004	35.001	103.040	3110	2.6 ± 0.2	47.6
26	dxh-11-ef005	35.023	102.974	2996	3.2 ± 0.3	59.1
27	dxh-11-ef006	35.056	102.988	2972	15.5 ± 0.8	593.4
28	dxh-11-ef007	35.069	102.990	3044	3.2 ± 0.4	47.6
29	dxh-11-ef008	34.931	102.864	3058	2.3 ± 0.6	19.8
30	dxh-11-ef009	34.911	102.865	3053	4.0 ± 0.4	15.6
31	dxh-11-ef010	35.031	102.823	2876	3.6 ± 0.3	55.2
32	dxh-11-ef011	34.984	102.777	2988	5.3 ± 0.4	130.8
33	dxh-11-ef012	35.022	102.824	2887	5.8 ± 1.0	175.6
34	dxh-11-ef013	35.048	102.831	2833	8.3 ± 0.8	241.9
35	dxh-11-ef016	35.091	102.917	2749	12.8 ± 1.0	809.5
36	dxh-11-ef017	35.136	102.849	2637	19.1 ± 1.0	1054.0
37	dxh-11-mf023	35.365	102.871	2309	37.2 ± 0.8	5212.5
38	dxh-11-mf024	35.365	102.884	2291	28.5 ± 1.4	5324.8
39	dxh-11-mf025	35.299	102.776	2424	31.7 ± 2.9	3849.1

$$W^* = 11.2 \left(1 - \frac{0.853}{\phi} \right) 4.5 \tag{9}$$

where W^* is a dimensionless transport rate and ϕ is a dimensionless transport stage. These two parameters are defined as follows:

$$W^* = \frac{(s-1)gq_b}{\rho_s (\tau/\rho_w)^{1.5}} \tag{10}$$

and

$$\phi = \frac{\tau^*}{\tau_r^*} \tag{11}$$

where s is the specific gravity of sediment (2.65), q_b is the mass transport rate of bed load per unit channel width (kg m^{-1} s^{-1}), ρ_s is the sediment density (2650 kg m^{-3}), ρ_w is the water density (1000 kg m^{-3}), $\tau = \rho_w gHS$ is the shear stress, and $\tau^* = \tau ((\rho_s - \rho_w)gD_{50})^{-1}$ is the dimensionless shear stress, where D_{50} represents the particle size for which 50% of particles are finer (Table 4). In equation (11) the term in the numerator, τ^*, refers to the dimensionless "bankfull" shear stress and the term in the denominator, τ^*_r, refers to the dimensionless "reference" shear stress that would produce a small but non-negligible transport rate. The

Table 4. Summary of the Daxia River Results

Field Number/Label	Latitude (deg)	Longitude (deg)	Elevation (m)	Drainage Area (km²)	Bankfull Discharge Q (m³ s⁻¹)	Channel Width W (m)	Channel Depth H (m)	Slope S	D_{84} (mm)	D_{50} (mm)	τ [a]	τ^* [b]	τ^*_r [c]	φ [d]	W^* [e]	q_b [f]	Q_b (kg s⁻¹) [g]
dxh-11-mf006/Q1	35.035	102.377	3202	39.31	2.2	5.8±0.3	0.30	0.0136	85	45	39.03	0.054	0.051	1.06	0.007	0.009	0.051
dxh-11-mf008/Q2	35.024	102.498	3333	60.65	1.7	4.0±0.2	0.30	0.0157	78	47	46.46	0.061	0.055	1.11	0.015	0.024	0.096
dxh-11-mf001/Q3	34.967	102.242	3424	103.48	3.8	8.0±0.4	0.33	0.0103	53	31	36.68	0.073	0.043	1.68	0.464	0.534	4.273
dxh-11-ef015/Q4	35.192	102.625	2878	387.75	5.5	7.2±0.4	0.38	0.0073	81	43	38.64	0.056	0.037	1.50	0.259	0.322	2.316
dxh-11-ef014/Q5	35.190	102.604	2860	533.09	8.7	9.4±0.5	0.38	0.0103	86	34	55.17	0.100	0.043	2.31	1.403	2.977	27.983
dxh-11-mf011/Q6	35.133	102.446	3021	751.74	8.3	11.2±0.6	0.48	0.0066	72	37	33.59	0.056	0.035	1.58	0.346	0.349	4.256
dxh-11-mf012/Q7	35.182	102.482	2956	1672.39	23.1	20.4±0.6	0.67	0.0060	78	46	43.17	0.058	0.034	1.70	0.489	0.718	14.352
dxh-11-mf021/Q8	35.221	102.812	2552	2111.43	56.7	31.2±1.6	0.81	0.0109	142	71	86.05	0.075	0.045	1.67	0.452	1.869	58.314
dxh-11-mf022/Q9	35.244	102.821	2499	3796.03	66.4	27.4±1.4	1.31	0.0049	103	49	68.55	0.086	0.032	2.73	2.072	6.089	127.869

[a] τ is the shear stress, $\tau = \rho_w g H S$.
[b] τ^* is the dimensionless shear stress, $\tau^* = \tau \left((\rho_b - \rho_w)g D_{50}\right)^{-1}$.
[c] τ^*_r is the critical shear stress, $\tau^*_r = 0.021 + 2.18S$, where r refers to the "reference" flow.
[d] φ is a dimensionless bankfull transport stage, $\phi = \frac{\tau^*}{\tau^*_r}$.
[e] W^* is a dimensionless transport rate, $W^* = 11.2\left(1 - \frac{0.853}{\phi}\right)^{4.5}$.
[f] q_b is the bed load transport rate per unit width, $q_b = \frac{W^* \rho_s(\tau/\rho_w)^{1.5}}{(s-1)g}$.
[g] Q_b is the transport capacity, $Q_b = q_b W$.

reference τ^*_r was estimated by using an empirical relation presented by *Mueller et al.* [2005], developed from an analysis of bed load transport measurements in 45 gravel bed rivers in western North America:

$$\tau^* = 0.021 + 2.18S \qquad (12)$$

where S is reach-scale channel gradient. Using the above definitions, equation (10) can be rewritten to determine the specific bed load transport rate (q_b, kg m⁻¹ s⁻¹) and the bed load transport capacity (Q_b, kg s⁻¹), assuming no limit to sediment supply:

$$q_b = \frac{W^* \rho_s (\tau/\rho_w)^{1.5}}{(s-1)g} \qquad (13)$$

$$Q_b = q_b W \qquad (14)$$

We also evaluated incision potential by developing reach-scale estimates of unit stream power and boundary shear stress [*Whipple and Tucker*, 1999]. Unit stream power is defined as the rate at which the potential energy per unit area of the river bed is lost by flow down the river slope. Assuming steady, uniform flow, unit stream power, ω (W m⁻²), can be calculated from

$$\omega = \rho_w g \frac{Q}{W} S \qquad (15)$$

A relation for boundary shear stress, τ_b (Pa), can be obtained by combining the Manning formula with the equation for water discharge:

$$\tau_b = \rho_w g \left(\frac{nQ}{W}\right)^{3/5} S^{7/10} \qquad (16)$$

where n is the Manning friction factor (assumed to be 0.04) [e.g., *Allen et al.*, 2013; *Snyder et al.*, 2000]. After formulating equations (5) and (6) and determining the reach-scale channel gradient (S), we solve equations (15) and (16) for a distribution of unit stream power and the boundary shear stress within the Daxia catchment.

4. Results

4.1. Stream Profiles

Analysis of channel profiles along the main tributaries of the Daxia River reveals the presence of knickpoints at elevations of ~2800–3200 m; these sit at distances between 110 and 130 km upstream of the junction of the Daxia and Yellow Rivers
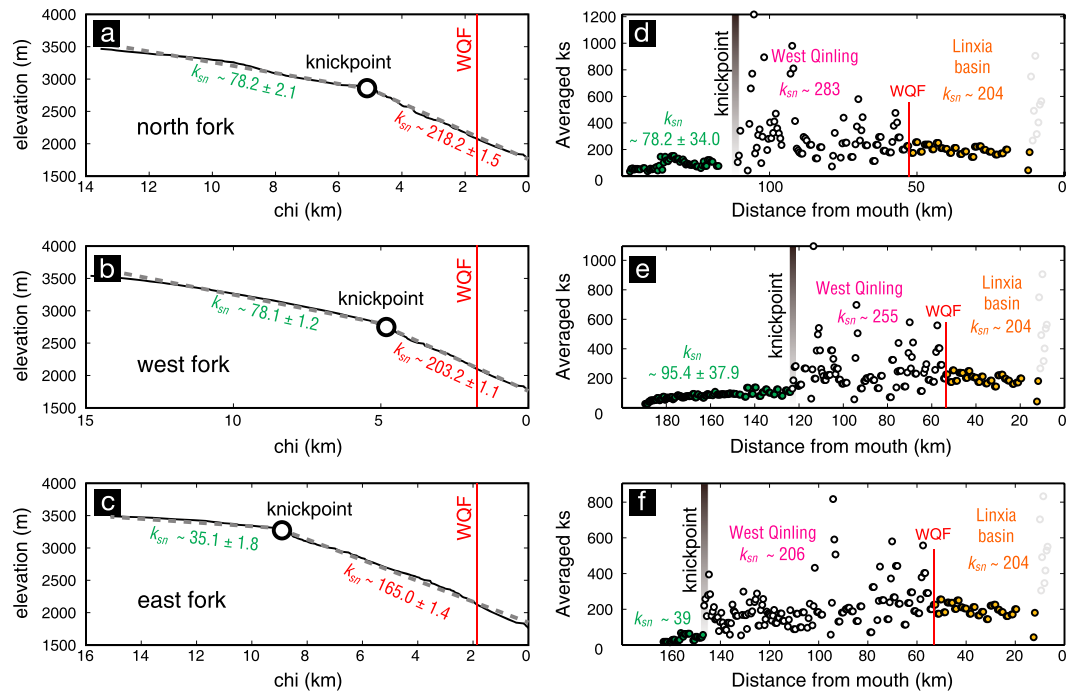
Figure 5. (a–c) Chi-elevation plot and normalized channel steepness (k_{sn}) values as a function of (d–f) distance from the river mouth for the three forks of the Daxia River. Knickpoints are recognized as abrupt changes in the slope of chi-elevation plots. Reach-averaged k_{sn} values derived from chi-plots and slope-area k_{sn} plots are also shown for comparison in Figures 5a–5c and in 5d–5f, respectively. Normalized steepness values are comparable for both chi-plot and slope-area analyses. Abnormally higher channel steepness ~0–10 km from the mouth (grey circles) is possibly due to the existence of a reservoir along the Yellow River. Difference in channel steepness is relatively subtle across the West Qinling fault into the Linxia basin (Figures 5d–5f).

(Figures 2 and 3). Knickpoints are associated with an abrupt change in the slope of chi-elevation plots (Figures 5a–5c) and thus bound portions of the channel network characterized by differences in channel steepness (Figures 5d–5f) ("slope-break" knickpoints) [*Kirby and Whipple*, 2012]. The position of these knickpoints is spatially coincident with the relatively sharp boundaries evident in maps of topographic slope and local relief (Figure 3) between a low-relief landscape in the upper watershed and high relief downstream (Figure 3b).

Channel reaches downstream of knickpoints are characterized by normalized steepness indices significantly greater ($k_{sn} > 200 \, m^{0.9}$) than those upstream ($k_{sn} < {\sim}100 \, m^{0.9}$) (Figure 5). Notably, the slope of the chi-elevation plot (Figures 5a–5c) yields similar values to the average normalized steepness index derived from analysis of slope-area plots (Figures 5d–5f), as has been shown in studies elsewhere [*Royden and Taylor Perron*, 2013]. Reach-averaged k_{sn} values, however, reveal a subtle difference in channel steepness across the West Qinling fault (Figures 5d–5f); channels draining the metasedimentary rocks south of the fault exhibit steepness values between ~200 and 280 $m^{0.9}$, whereas the trunk channel in the Tertiary sandstones of the Linxia basin is ~200 $m^{0.9}$. To explore the distribution of channel steepness throughout the watershed, we calculated k_{sn} values at 500 m intervals along the channel network and interpolated the results (Figure 6). This visualization illustrates the sharp contrast in channel steepness across knickpoints; average k_{sn} values below knickpoints are up to 7 times greater than average values upstream (Figure 6). Similarly, average k_{sn} values along channels developed in the Tertiary rocks of the Linxia basin are low, similar to those above knickpoints, despite the high rates of incision (Figure 6).

The distribution of channel steepness values and the presence of knickpoints highlight two important characteristics of the fluvial network. First, knickpoints along the main tributaries of the Daxia River are located well upstream of the lithologic boundary between the Linxia basin and the metasedimentary rocks of the West Qinling (Figures 2b and 5). Given that these low-grade metasedimentary rocks are relatively homogeneous (Figure 2a) [*BGMR Gansu*, 1989], this observation confirms our inference that knickpoints
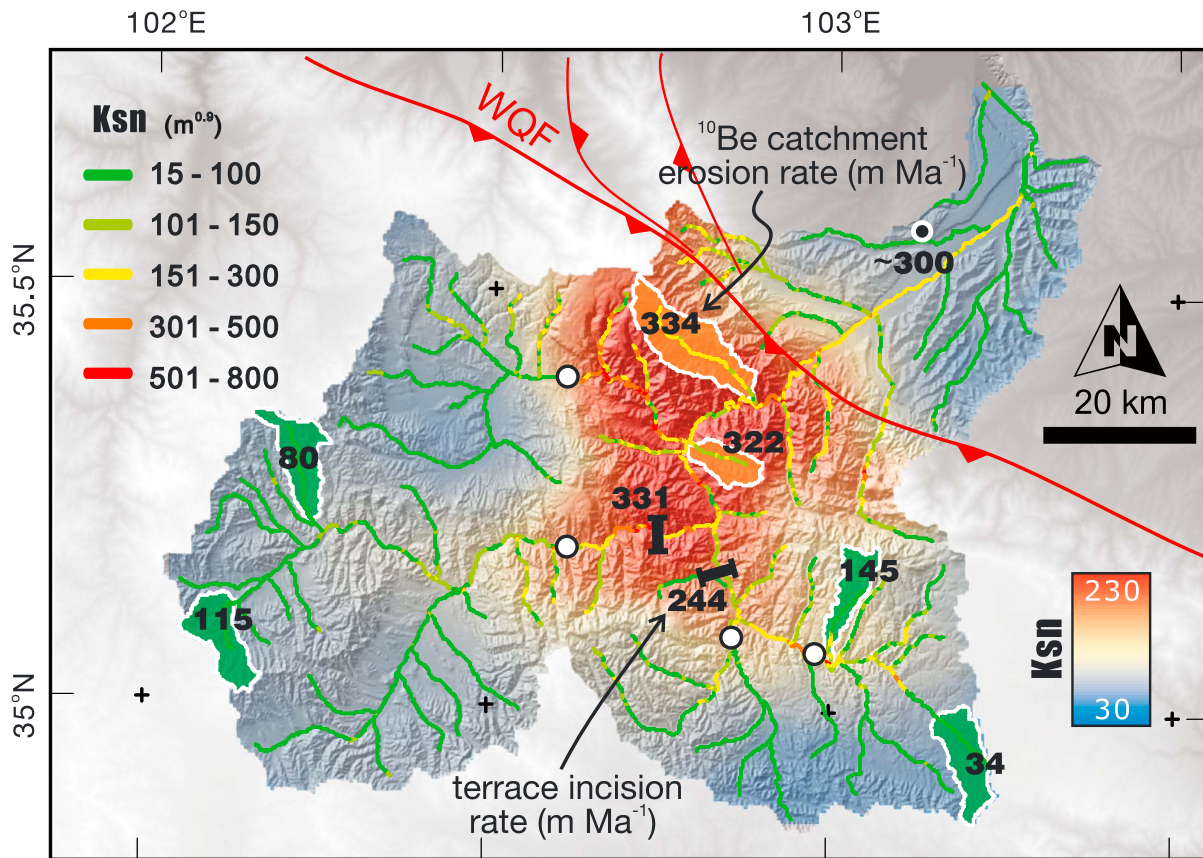
Figure 6. Channel steepness and rates of catchment erosion/terrace-site incision in the Daxia River catchment. To easily visualize the sharp contrast of the highest channel steepness downstream of the knickpoints (white dots), interpolation of rasterized channel steepness values was sampled at 500 m intervals along the channel network. Sampled catchments are color-coded to highlight their distribution downstream (orange) and upstream (green) of the knickpoints. Incision rates are only shown from lower terraces (Table 2). Also shown is ~300 m Ma^{-1} of long-term incision rate from the ~1.7 Ma old river terraces (~500 m above present Daxia River) at Wangjiashan (W in Figure 2a) within the Linxia basin [*Li et al.*, 1997].

represent the position of a migrating wave of channel adjustment, rather than features anchored to resistant substrate. Second, the main stem Daxia River remains steep even within the Tertiary sediments of the Linxia basin, downstream of the West Qinling fault, with k_{sn} values ~200 m$^{0.9}$ (Figures 5d–5f and 6). These values are significantly greater than those along tributaries developed in the Tertiary basin sediments (Figure 6), all of which have k_{sn} values <100 m$^{0.9}$. We will return to this observation in the discussion, but we note that this behavior is consistent with the expectation that gradients along the main stem may be set by the transport of coarse sediment from resistant rocks upstream rather than detachment of local substrate [e.g., *Tucker and Whipple*, 2002; *Duvall et al.*, 2004].

4.2. Differences in Erosion and Channel Incision Rate

The concentrations of ^{10}Be in modern sediment from tributary watersheds imply an approximately tenfold range in erosion rates across the Daxia drainage basin (Figure 6). For the six catchments we sampled, erosion rates vary over a range of ~30–330 m Ma^{-1} (Table 1 and Figure 6). The samples from the catchments above the knickpoints yield relatively low rates, between 34 and 145 m Ma^{-1} with an average of ~93 m Ma^{-1} (Table 1 and Figure 6). Below knickpoints, however, catchments in the high-relief landscape are eroding at rates of 320–340 m Ma^{-1} (Table 1 and Figure 6).

The pattern of watershed-average erosion rates is corroborated by the rate of fluvial incision determined from dating of strath terraces. Two relatively continuous series of strath terraces (TS1 and TS2) extend along the Daxia River main stem for ~10–15 km downstream of the knickpoints (Figure 6). Dating of alluvial sands interbedded with gravel on the terrace tread by optically stimulated luminescence (OSL) suggests that these
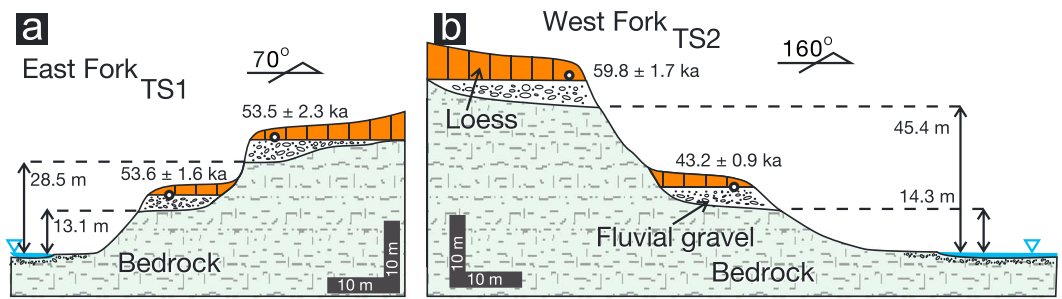
Figure 7. Strath terrace cross section and OSL ages for East and West Forks of the Daxia River (Table 2). OSL samples were taken within loess and sand ~20 cm above the gravel on the terraces. Strath heights above the active river channel were surveyed with a hand-held TruPulse 200 laser rangefinder. Possibility exists for two levels of TS 1 as a fill terrace due to their similar ages.

treads were occupied between ~43 and 60 ka (Figure 7 and Table 2). Farther downstream, within the Linxia basin, a single, isolated strath terrace (TS3) yielded a late Pleistocene age of ~11 ka (Table 2). Dividing by the strath bedrock elevation above the present active channel, the average late Pleistocene incision rates are 530–760 m Ma^{-1} for the higher terraces and 240–330 m Ma^{-1} for the lower ones (Table 2), consistent with the catchment-average erosion rates below the knickpoints (Figure 6). The exception occurs in the Linxia basin at terrace TS3, which lies ~13 m above the modern river and is dated at ~11 ka (Table 2). Here the incision rate is quite high at ~1200 m Ma^{-1}, almost 3–4 times higher than the rates derived from both catchment-average erosion rates and terrace incision rates (Table 2). However, because this terrace is the lowest (youngest) observed, we suspect that this rate does not reflect the long-term average in the Linxia basin. Models of terrace formation modulated by sediment flux variations across glacial-interglacial cycles [e.g., *Hancock and Anderson*, 2002] suggest that the incision rates measured over the full duration of terrace cutting during lateral planation and postabandonment incision approximate the rates of base-level fall. Similar reasoning has been used to explain high rates of incision from the lowest terraces in the Olympic Mountains of western North America [*Wegmann and Pazzaglia*, 2002]. Overall, fluvial incision rates of ~300 m Ma^{-1} in reaches below the knickpoints appear to be consistent with the long-term average incision rate inferred from the height and age (~1.7 Ma) of the top of basin fill [*Li et al.*, 1997].

Despite our limited data set from six tributary catchments (Figure 6), erosion rates appear to be positively correlated with average channel steepness, slope, and local relief (Figure 8), consistent with previous studies in eastern Tibet [*Harkins et al.*, 2007; *Ouimet et al.*, 2009; *Kirby and Ouimet*, 2011; *Kirby and Harkins*, 2013]. Coordinated downstream increases in slope distribution (Figure 4a), local relief (Figure 4b), and channel steepness (Figure 5) suggest that elevated erosion rates between the knickpoints and the West Qinling fault are consistent with downstream increases in sediment input into the drainage system associated with transient channel incision.

4.3. Reconstructing Incision From Channel Profile Geometry

To estimate the amount of incision recorded by transient river profiles, we follow previous workers [*Kirby and Whipple*, 2012] and utilize the average normalized channel steepness (~20–80 m$^{0.9}$) from relict channel segments above knickpoints (Figure 6) to predict the former distribution of downstream gradients (equation (3)). This assumes that rivers were once graded to the top of the terrestrial fill in the Linxia basin and that catchment areas have not varied significantly through time. Variations in the steepness of channel profiles upstream of knickpoints suggest that the "relict" landscape was not entirely flat but likely had some initial relief. To account for this, we estimate the amount of channel lowering upstream of knickpoints that would have occurred during the 1.7 Ma duration of transient incision by using average erosion rates from our cosmogenic isotope measurements. We exploit the relationships between mean basin slope, local relief, channel steepness k_{sn}, and erosion rate (Figure 8) and estimate the average erosion rates that would be associated with the upstream reaches of all three forks of the Daxia River watershed. Essentially, this amounts to assuming that the modern relationships can be extrapolated back in geologic time; although such an assumption may be incorrect, similar methods have been used to reconstruct landscape evolution elsewhere [*Schildgen et al.*, 2012; *Miller et al.*, 2013].
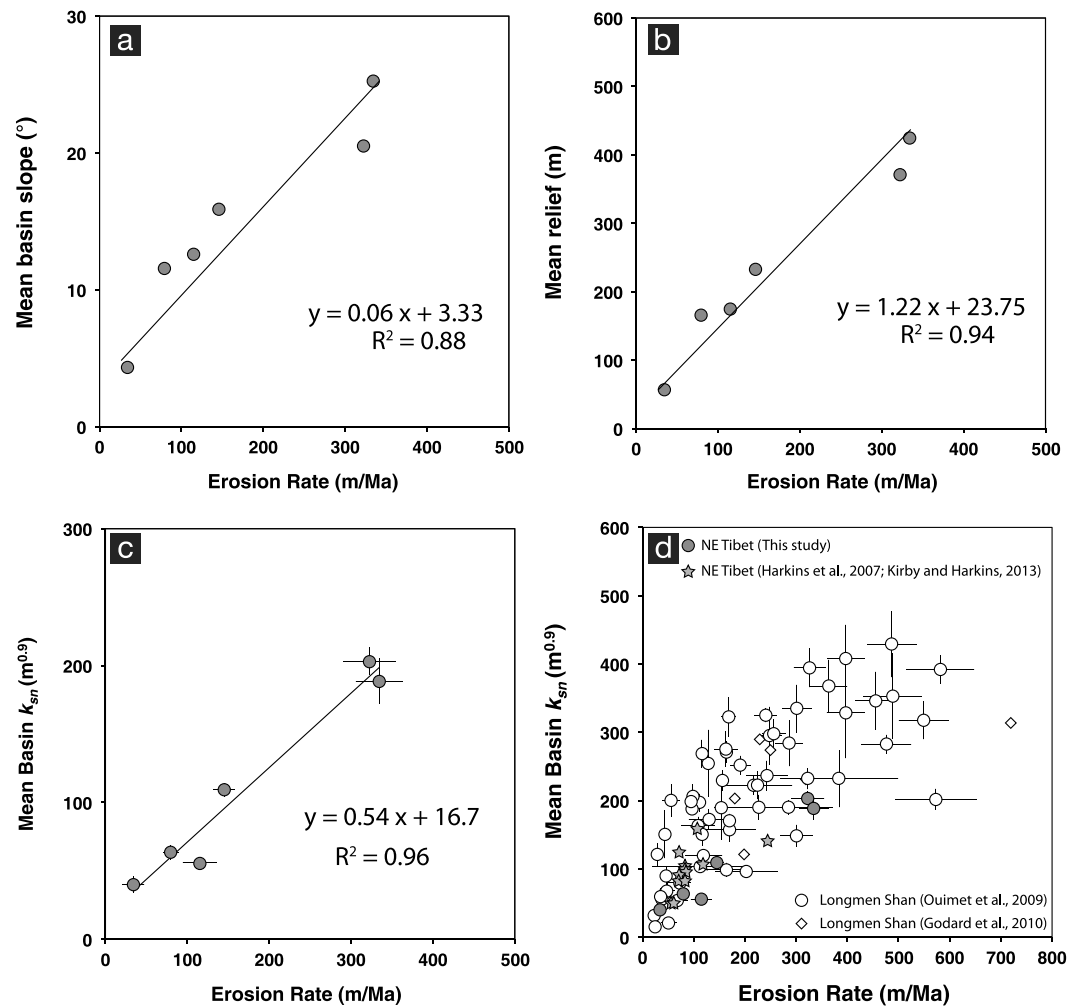
Figure 8. Relationships of catchment erosion rates and (a) mean basin slope, (b) local relief, and (c) channel steepness. (d) Functional relationship between erosion rates and mean basin channel steepness index (k_{sn}) compiled from studies in eastern and northeastern Tibet. Most watersheds are underlain by greywacke (primarily Triassic flysch), schist, and other sedimentary rocks.

Our results suggest that the amounts of lowering along the relict profiles of the East Fork, North Fork, and South Fork are ~60 m, 200 m, and 250 m, respectively (Figure 9). The paleolongitudinal profile projections suggest that the total depth of incision was in the range of ~800–850 m. Notably, the accounting of upstream lowering yields relatively close agreement among the three individual tributary profiles (Figure 9). However, the estimate of 800 m of incision is ~300 m greater than the amount of incision inferred from previously dated Cenozoic basin fill section at the Wangjiashan site [*Li et al.*, 1997; *Fang et al.*, 2003]. We will return to this point in the discussion below.

4.4. Scaling Relationships of Channel Geometry and Bed Load Transport Capacity

The results from our field surveys allow us to evaluate the reach-scale channel characteristics of the Daxia River and its tributaries. Figure 10 shows a series of plots depicting downstream trends in channel properties above and below knickpoints. The properties measured in the field include channel width, depth, slope, and grain size (*W*, *H*, *S*, and *D*, respectively); the properties derived from field measurements are those needed to calculate bed load transport capacity, i.e., dimensionless shear stress and bed load transport stage (τ^* and ϕ, respectively). Figure 10a shows relations between channel width and drainage area, with points color-coded by location. Above the knickpoints, channel width increases at a slightly higher rate along the West Fork (blue) than the East Fork (red), but the difference is small. Below the knickpoints (green), width increases at
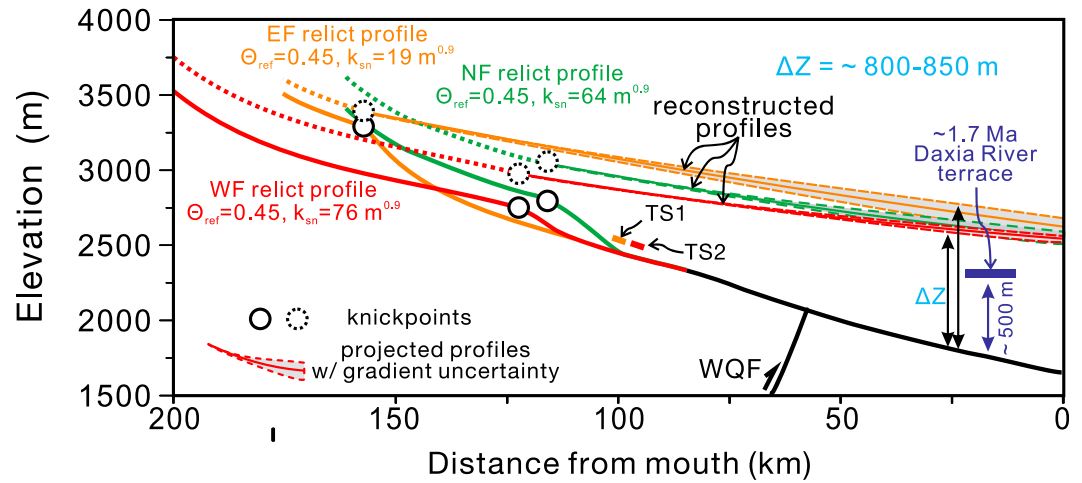
Figure 9. Present longitudinal profiles and paleolongitudinal profile reconstructions of the three Daxia River forks, following *Kirby and Whipple* [2012] and *Miller et al.* [2013]. The gray-shaded envelopes with dashed outlines are upper and lower limits for the reconstructed profiles. Total incision ($\Delta Z = 800$–850 m) in the past 1.7 Ma was estimated by projecting the upstream relict channel profile into the Linxia basin. Corrections to the profile projections were made by accounting for the landscape lowering above the knickpoints in the past 1.7 Ma.

a somewhat slower rate, but the relation is weaker due to small sample size and a limited range of drainage areas (Figure 10a). The entire data set of 48 sites can be fit by a single regression equation (gray), with $k_w = 0.8 \times 10^{-3}$ m$^{1.04}$ and $a = 0.48$, suggesting a continuous scaling of width through the major knickpoints. Notably, the value of the exponent (~0.5) is consistent with the results from previous studies of channels that are self-formed [*Emmett*, 1975; *Wohl and David*, 2008], as well as channels that are steadily incising through bedrock [*Montgomery and Gran*, 2001; *Snyder et al.*, 2003a, 2003b; *Duvall et al.*, 2004; *Whipple*, 2004].

The scaling relation between discharge and drainage area (Figure 10b) is based on fewer points—the nine sites where bankfull discharge was estimated from channel properties; however, these data likewise exhibit a power law scaling (equation (6)), with $k_q = 2.0 \times 10^{-6}$ m$^{1.44}$ s^{-1} and $b = 0.78$ (Figure 10b). Discharges estimated at sites below the major knickpoints are somewhat higher than the overall trend, but the exponent (~0.8) is typical of discharge-drainage area relations developed in studies of gravel bed channels in other settings [e.g., *Emmett*, 1975; *Mueller and Pitlick*, 2005, 2013].

Figures 10c–10f show scaling relations for bankfull width, depth, channel gradient, grain size, shear stress, and bed load transport capacity, all plotted as functions of bankfull discharge. In Figures 10c–10e, the regression relations have been fit by using only data collected upstream of the knickpoints and the best fit lines have been extrapolated through the knickpoints to assess whether data from reaches within or below these areas deviate appreciably from the overall trends. One caveat to this analysis is the potential for spurious correlation among variables because Q_b is estimated from channel geometry, slope, and grain size. This fact and the small sample size limit the explanatory power of the regression relations, but the fitted lines serve as a basis for comparison with previous work.

The relations presented in Figure 10c show that the trends in depth and slope defined by the data collected upstream of the knickpoints are broadly consistent with trends reported in previous studies of alluvial channels ($H \propto Q^{0.24}$ and $S \propto Q^{-0.41}$) [*Andrews*, 1984; *Hey and Thorne*, 1986; *Pitlick and Cress*, 2002; *Parker et al.*, 2007]. However, at sites below the knickpoints, the measurements of depth and slope plot slightly above the extrapolated trends, consistent with the increase in channel steepness, k_{sn}, below knickpoints (Figures 5 and 6). The measurements of bed surface grain size also plot above the extrapolated trends (D_{50} and D_{84}; Figure 10d) and likely reflect an increase in sediment supply from the steeper parts of the basin below the knickpoints (Figure 3). To understand how these differences influence bed load transport capacity, we turn to Figure 10e, which shows downstream relations for reach-average bankfull shear stress, τ, and dimensionless shear stress, τ^*. As in the previous plots, the trends shown here are defined by data collected upstream of the knickpoints, then extrapolated to lower reaches. The relation for shear stress defined by values above the knickpoints is negative ($\tau \propto Q^{-0.18}$) and consistent with trends in alluvial rivers where slope commonly
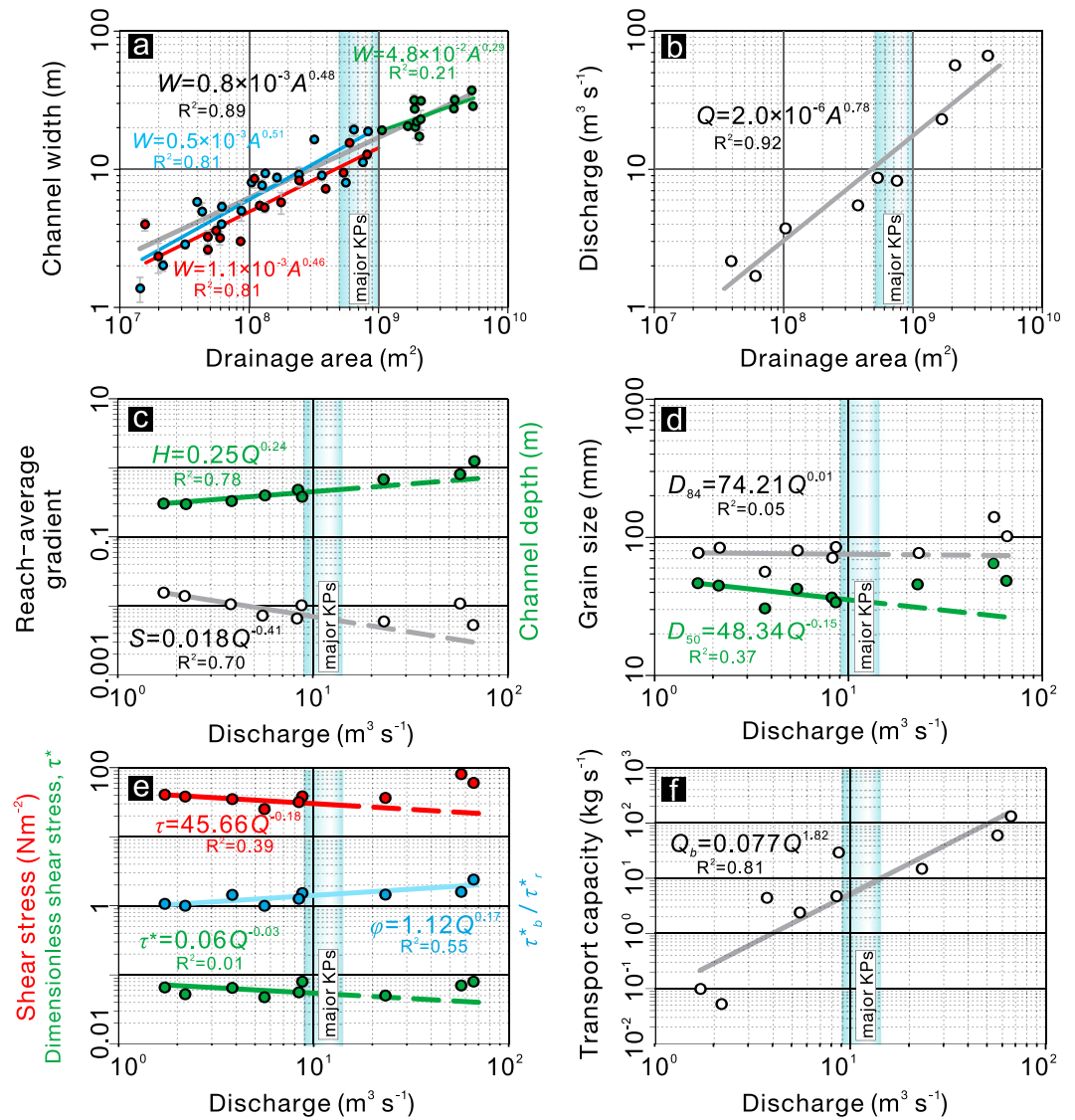
Figure 10. Bankfull scaling relationships of channel width, (a) discharge, and (b) drainage area (blue = West Fork, red = East Fork, green = main stem downstream of major knickpoints, gray curve = average fit of all data) and relation of (c) discharge with channel depth and reach-average gradient, (d) grain size, shear stress, dimensionless transport stage, (e) dimensionless shear stress, and (f) bed load transport capacity. Note that Figure 10a presents the measurements of the channel width at 48 sites, but Figures 10b–10f only show nine selected sites (see Figure 2b for the fieldsite locations). Regressions in Figures 10c–10e are fit by using data upstream of the knickpoints to assess whether the downstream data deviate appreciably from the overall trends. All hydraulic variables are for bankfull flow.

decreases faster than depth increases [*Andrews*, 1984; *Hey and Thorne*, 1986]. The observation that depth and slope are both higher downstream of the knickpoints leads to an overall trend where the bankfull shear stress actually increases downstream. That trend is approximately balanced by the increase in median grain size, D_{50}, such that the variation in bankfull dimensionless shear stress across the knickpoints is negligible ($\tau^* \propto Q^{-0.03}$).

The effect of these inter-related trends on sediment flux is illustrated in the plots of bankfull bed load transport stage, ϕ (Figure 10e), and bankfull bed load transport capacity, Q_b (Figure 10f). In this case, we fit values upstream and downstream of the knickpoints with a single relation; we did this in order to include the effects of potential interactions among variables (depth, slope, and grain size) that determine basin-wide trends in bed load transport stage and transport capacity. The results show that the values of bed load transport stage, ϕ, can be fit by a single regression equation, with no clear variation in residuals above and below

knickpoints. The relation for bankfull bed load transport capacity exhibits more scatter than any of the other relations, but the values follow a well-defined trend with Q_b increasing downstream to the 1.8 power of Q (Figure 10f). An exponent of 1 would imply that water and sediment were being transported through the basin in exact proportion to each other. Our results suggest that this is not the case in the Daxia River basin: the nonlinear increase in Q_b is consistent with a river system that is incising downstream in response to a forced change, which in this case involves base-level lowering.

4.5. Spatial Patterns of Shear Stress and Stream Power

In addition to the nine sites at which shear stress is estimated from field data (Figure 10e), we solve equations (15) and (16) for catchment-scale distributions of unit stream power and basal shear stress by using the averaged (~1 km) channel gradient (S) calculated from the ~90 m resolution DEM. Stream power and shear stress along the Daxia River and its major tributaries clearly show a downstream increase (Figure 11). Above the knickpoints, stream power along the channels is for the most part less than $200\,W\,m^{-2}$ but locally increases to more than 1000, reaching $>2000\,W\,m^{-2}$ downstream of the knickpoints (Figure 11a). Similar to the pattern of stream power, boundary shear stress remains relatively low (less than $150\,N\,m^{-2}$) upstream of the knickpoints and increases to $>300\,N\,m^{-2}$ below the knickpoints (Figure 11b). There exist a few exceptions to this pattern: some channel segments show high stream power and shear stress above the knickpoints, for example, ~15–20 km upstream of the knickpoint along the West Fork. We suspect that this reflects either local lithologic differences between Cenozoic sediments and bedrock or possibly erodibility contrasts along antecedent faults within the basement rocks (Figure 2a). Within the Linxia basin, the main stem of the Daxia always has greater stream power and higher shear stress than its adjacent tributaries (Figure 11), consistent with its higher normalized steepness (Figures 5 and 8d–8f).

5. Discussion and Implications

### 5.1. Transient Landscape of the Daxia River: A Response to Base-Level Fall

Our geomorphic analyses confirm the notion that the present landscape of the Daxia River in the northeastern Tibetan Plateau is in a transient state, such that slowly eroding, low-relief topography in the headwater regions is separated from more rapidly eroding, high-relief topography by migrating knickpoints along the channel network. The boundary between these two domains is present upstream of the West Qinling fault and does not appear to simply mark exhumation of a pre-existing contrast in rock erodibility (Figures 5 and 6). Our results are likewise consistent with studies of incision along the main stem of the Yellow River, in the Anyemaqen range, where knickpoints are developed well upstream of deeply incised basin sediments [e.g., *Harkins et al.*, 2007].

To evaluate the consistency of knickpoint propagation along the Yellow River and Daxia River, we explored a simple knickpoint recession model that considers the behavior of a detachment-limited fluvial system [*Berlin and Anderson*, 2007]. Under the assumption that channel incision rate is linearly dependent on local channel slope, the stream power formulation for detachment-limited incision [e.g., *Whipple*, 2004] predicts that the migration rate of knickpoints, dx/dt ($m\,a^{-1}$) is a function of upstream drainage area, A (m), raised to a dimensional constant, m, and an erodibility coefficient, K ($m^{1-2m}\,a^{-1}$) [*Rosenbloom and Anderson*, 1994; *Whipple and Tucker*, 1999; *Berlin and Anderson*, 2007]:

$$\frac{dx}{dt} = KA^m \tag{17}$$

Using a similar approach, *Harkins et al.* [2007] suggested that tributary channel profiles in the Yellow River watershed within the Anyemaqen Shan are adequately described by using erosion coefficients K that range between 3.7×10^{-6} and $9.5 \times 10^{-5}\,m^{0.5}\,a^{-1}$ [*Harkins et al.*, 2007].

Our analysis of knickpoint position within the Daxia River appears to be consistent with the regional propagation of knickpoints up the Yellow River. Along the main stem of the Yellow River, incision propagated up the trunk channel at average rates of ~350 km Ma^{-1} [*Craddock et al.*, 2010]. Given that the initiation of incision across the Linxia basin occurred at ~1.7 Ma [*Li et al.*, 1997; *Fang et al.*, 2003], the present position of knickpoints along the Daxia River implies that the upstream propagation of knickpoints occurred at an average rate of ~70–80 km Ma^{-1} (Figure 2). Using equation (17), we can estimate the average erodibility (K)
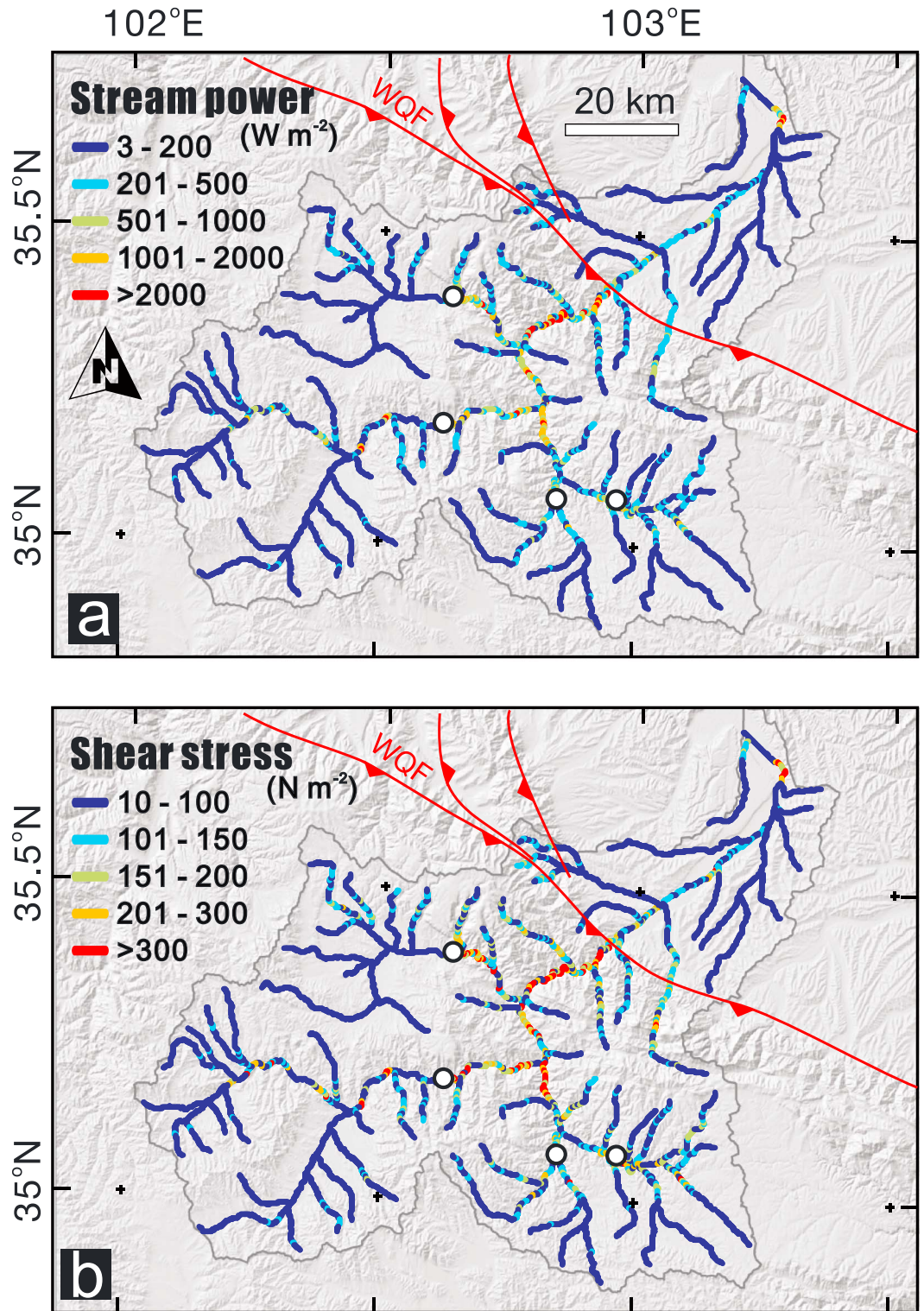
Figure 11. Bankfull estimates of unit stream power and shear stress across the Daxia River catchment. Transport capacity increases downstream of the knickpoints (white dots).

required for knickpoints to transit this distance at this rate. Along the Yellow River, the average rate of knick-point retreat (dx/dt) is ~350 km Ma^{-1} and the contributing drainage basin area upstream of the knickpoint at Zhe Qu [*Harkins et al.*, 2007] is 9.8×10^{11} m^2. Considering a range of values for m between 0.4 and 0.5, consistent with previous work [*Harkins et al.*, 2007], we estimate an erosion coefficient K of 1.1×10^{-6} m^0 a^{-1} to 1.4×10^{-5} m$^{0.2}$ a^{-1}. Following the same reasoning along the Daxia River (with dx/dt = ~70–80 km Ma^{-1} and drainage basin areas of 9.0×10^8 m^2 for NF, 1.9×10^9 m^2 for WF, and 6.5×10^8 m^2 for EF), we find a range of erosion coefficient K of 1.7×10^{-6} m^0 a^{-1} to 2.3×10^{-5} m$^{0.2}$ a^{-1}. Although this calculation is admittedly simple, the consistency of these results suggests that, to first order, the incisional wave is behaving as expected for a simple, detachment-limited model of fluvial incision.

Of course, it is likely that rates of downcutting during migration of this incisional wave would have varied with time, as rapid initial incision drove excavation of Tertiary sedimentary rocks in the Linxia basin. The height of terraces near the Wangjianshan section suggests incision rates of ~1 km Ma^{-1} in the first few 100 ka following the onset of incision [*Li et al.*, 1997], and the recycling of conglomerate clasts into terraces along the Yellow River at Lanzhou [*Hu et al.*, 2011] likewise requires rapid exhumation into Pliocene conglomerates at the top of the basin fill. Similarly, incision rates measured over the past 30–100 ka immediately downstream of knickpoints along tributaries of the upper reaches of the Yellow River range from 1 to 2 km Ma^{-1} [*Harkins et al.*, 2007].

One interesting aspect of our results is the difference in the amount of incision across the Linxia basin inferred from our reconstruction of former river profiles and that estimated from preserved terraces. The latter is suggested to be ~500 m, measured from a 1.7 Ma terrace tread of the Daxia River [e.g., *Li et al.*, 1997], whereas our reconstruction suggests that it may be closer to ~800 m. Both the catchment-averaged erosion rates and incision rates implied by strath terraces suggest an average rate of incision of 300 ± 50 m Ma^{-1} for the region of the watershed below knickpoints. At these rates, 500 m of incision would be accomplished in ~1.6 Ma; they are entirely consistent with independent estimates of the age of the highest terrace [*Li et al.*, 1997]. It is possible, therefore, that the additional 300 m suggested by profile reconstruction implies a component of differential rock uplift between the plateau and the basin during the past ~2 Ma.

5.2. Hydraulic Scaling of the Daxia River: Transient Incision Without Narrowing

One intriguing aspect of our results is that the hydraulic geometry of the Daxia River in the northeastern Tibetan Plateau maintains a relatively uniform scaling of channel width across the transition from low to high incision rates (Figure 10a). Measurements of width taken above and below knickpoints form a continuous trend, with width increasing as approximately the square root (a ~0.5) of drainage area. These observations contrast with the notion that channels generally narrow in response to base-level fall [*Lavé and Avouac*, 2000; *Attal et al.*, 2008, 2011; *Whittaker et al.*, 2007b, 2008] and/or spatial gradients in uplift rate [*Duvall et al.*, 2004; *Yanites et al.*, 2010; *Kirby and Ouimet*, 2011]. Our analysis of the hydraulic geometry of the Daxia River suggests that channel width can, at least in some circumstances, maintain a "typical" scaling across a three-fold to fivefold increase in incision rate (Figure 10a). These findings are similar to other studies in coastal California [*Snyder et al.*, 2003b; *DiBiase et al.*, 2010], both of which observed no significant difference in channel width in basins experiencing order of magnitude differences in erosion and/or uplift rate.

At present, most of our knowledge of channel narrowing comes from settings with high uplift/incision rates (>500 m Ma^{-1}, even >5000 m Ma^{-1}); these include the mountain ranges of coastal California [*Snyder et al.*, 2003a; *Duvall et al.*, 2004], the southern Alps of New Zealand [*Amos and Burbank*, 2007], the Hsuehshan Range in central Taiwan [*Yanites et al.*, 2010], the eastern margin of the Tibetan Plateau [*Kirby and Ouimet*, 2011], and the rapidly growing folds in the foreland of the Himalaya [*Lavé and Avouac*, 2000; *Allen et al.*, 2013]. Under relatively rapid uplift/incision rates, channels were observed to be narrower than predicted by a simple scaling (Table 5; $W \propto A^{<0.4}$). However, numerous studies show that channel width in drainage basins undergoing relatively low uplift rates (i.e., <300–500 m Ma^{-1}) exhibits scaling relations consistent with those from alluvial channels (Table 5; $W \propto A^{0.5}$) [*Snyder et al.*, 2003a; *Tomkin et al.*, 2003; *Whittaker et al.*, 2007a, 2007b; *Kirby and Ouimet*, 2011; this study]. These observations hint at the possibility that the rate of channel incision (and/or uplift) governs the adjustment of channel geometry. In regions with relatively high uplift rates (>300 m Ma^{-1}), channel widening cannot keep pace with forced changes in slope. However, in regions that are eroding relatively slowly (<300 m Ma^{-1}), there is more time for the channel to adjust and we

Table 5. Summary of the Channel Width Response to Uplift/Erosion Rates

	Uplift/Erosion Rate (m Ma^{-1})			
Location	Minimum	Maximum	Channel Width Description	Reference
	Higher Uplift/Erosion Rate Region			
Siwaliks Hills, Central Nepal	4,000–8,000	10,000–15,000	Channels narrow, no measurements	*Lavé and Avouac*, 2000
Mendocino Triple Junction, California	500	~4,000	Variable channel widths, $W \sim A^{0.2-0.6}$	*Snyder et al.* [2003a, 2003b]
Santa Ynez, California	~750	~5,000	Channels narrow, $W \sim A^{0.4}$	*Duvall et al.* [2004]
Yarlung Tsangpo, China			Channels narrow, $W \sim A^{3/8} S^{-3/16}$	*Finnegan et al.* [2005]
Southern Alps, New Zealand		1,000–2,000	Channels narrow across fold	*Amos and Burbank*, [2007]
Rio Torto, Central Italy	~300	1,000	Overall, $W \sim A^{0.45}$	*Whittaker et al.* [2007a, 2007b]
Peikang River, Central Taiwan	~100–200	~600–1,000	Channels narrow across faults	*Yanites et al.* [2010]
Central Longmen Shan, China	500	1,000–2,000	Channels narrow, $W \sim A^{0.1-0.3}$	*Kirby and Ouimet*, [2011]
Siwalik Hills, northwest India	~6,900	~14,000	Channels narrow across fold	*Allen et al.* [2013]
	Lower Uplift/Erosion Rate Region			
Clearwater River, Washington	~100	~900	Variable channel widths, $W \sim A^{0.42}$	*Tomkin et al.* [2003]
Fosso Tascino, Central Italy	~350		$W \sim A^{0.55}$	*Whittaker et al.* [2007a, 2007b]
Valleluce River, Central Italy	0–300		$W \sim A^{0.51}$	*Whittaker et al.* [2007a, 2007b]
Northern Longmen Shan, China		<500	No obvious narrowing, $W \sim A^{0.57}$	*Kirby and Ouimet*, [2011]
Spanish Baetic Cordillera, Spain	15	250	No channel width data	*Bellin et al.* [2014]
Daxia River catchment, China	~80	~350	No obvious narrowing, $W \sim A^{0.48}$	This study

therefore observe trends in width that are consistent with a global scaling relation where $W \propto A^{0.5}$ [*Leopold and Maddock*, 1953; *Wohl and David*, 2008]. Lithology will also influence rates of width adjustment, whereby rivers that are working their way through erodible rock types, as is the case in the lower Daxia River basin, have more freedom to adjust their hydraulic geometry, even if erosion rates are relatively low.

One variable that is often left out of the discussion of channel adjustments in incising rivers is grain size, D. In addition to discharge, grain size exerts a first-order control on channel slope and thus strongly influences bed load transport capacity. In the Daxia River, the bed surface grain size remains relatively coarse downstream of knickpoints in spite of a threefold to sevenfold increase in water discharge (Figure 10d); this trend presumably reflects an increase in sediment supply from the steeper, central parts of the basin. The supply of coarse particles appears to be sufficient to replenish sediment worn down by abrasion, which could explain why high channel slopes ($S > 0.005$) persist far downstream of knickpoints (Figure 10c). Notably, gradient remains high along the main stem channel but not on the tributaries downstream of the fault (Figure 6), suggesting that a sustained supply of coarse sediment from hillslopes pushes the system toward transport-limited gradients [*Duvall et al.*, 2004; *Attal and Lavé*, 2006; *Attal et al.*, 2015]. The net effect of the higher slopes is for the river to maintain a high bed load transport capacity, which might drive further incision independent of any substantial changes in width or depth.

It has been suggested that the adjustment of channel width and slope to imposed rates of base-level fall is also strongly dependent on the ratio of sediment supply to transport capacity; in theory, this ratio represents competing effects of "tools" that can erode the bed versus the sediment "cover" that can protect it [*Wobus et al.*, 2006a; *Turowski et al.*, 2007; *Cowie et al.*, 2008; *Yanites and Tucker*, 2010; *Attal et al.*, 2015]. Models developed to simulate these effects show that, as drainage area increases, channels become increasingly cover-dominated; consequently, a greater fraction of the available shear stress goes into transporting the sediment supplied and less into eroding the bed [*Turowski et al.*, 2007; *Yanites and Tucker*, 2010]. In addition, there appears to be a threshold in bed cover/erosion rate, below which channel geometry is insensitive to the imposed base-level fall. The results presented by *Turowski et al.* [2007] and *Yanites and Tucker* [2010] suggest that this threshold lies somewhere between 300 and 1000 m Ma^{-1}, with the lower limit being similar to erosion rates in the lower Daxia River basin. We would describe the lower reaches of the Daxia River as cover-dominated but in the realm of low erosion rates where channel geometry is determined by factors other than the rate of uplift or base-level fall.

5.3. Interpreting Knickpoints in a Transient Landscape: Implications of Channel Response

Our reach-scale observations along the Daxia River reveal a hydraulic scaling similar to alluvial rivers and a downstream increase in transport capacity, suggesting that the present-day state is close to a transport-limited condition. However, the profile of the main stem Daxia River and tributaries exhibit prominent

knickpoints that are associated with systematic differences in channel steepness and sustained differences in erosion rate. These observations suggest channel steepening in response to imposed base-level fall, consistent with the predictions of detachment-limited models [e.g., *Kirby and Whipple*, 2012]. Moreover, the rate of upstream knickpoint migration along the Daxia River appears to be consistent with that previously determined along the main stem Yellow River [*Harkins et al.*, 2007], again suggesting that a simple, detachment-limited rule adequately describes the evolution of river profiles over the ~1.7 Ma duration of the transient response.

One potential explanation for these apparent differences in channel morphology is that the current alluvial state of the bed and banks may not be representative of the conditions during incision [e.g., *Howard*, 1998]. Given that the initial wave of incision was likely characterized by rapid (>1 mm/yr) lowering of the channel bed [e.g., *Harkins et al.*, 2007], channel incision may have outpaced the rate of sediment supply immediately following base-level fall. This could have forced the system to behave near the detachment-limited end of the spectrum. As incision proceeded, however, and hillslope sediment supply increased from the watershed below the knickpoints, the system may have been driven toward a more transport-limited condition. Such behavior is characteristic of models that incorporate the effects of sediment as cover and tools in bedrock incision [e.g., *Gasparini et al.*, 2007].

It is also possible that climatically modulated variations in sediment supply may have affected the entire watershed, such that the present-day alluvial cover on the bed may not be representative of the conditions during times of bedrock incision [e.g., *Howard*, 1998; *Hancock and Anderson*, 2002]. Although the region was subjected to changes in both moisture and dust deliveries during glacial-interglacial cycles [e.g., *An et al.*, 2015], how these may have impacted local sediment production and transport from hillslopes to channels is largely unknown. It may be that periods of low sediment yield enable excavation of sediment from the bed and attack of the underlying bedrock, such that the morphology of the system reflects detachment-limited incision that is punctuated in time by periods of reduced erosive potential.

Reconciling the presence of slope-break knickpoints that separate distinct regions of increased channel steepness and erosion rate from "relict" landscapes with the hydraulic geometry relations that we have presented poses a challenge for models of transient evolution of fluvial systems. As noted previously, the main stem of the Daxia River remains steep across the boundary between the metasedimentary rocks of the West Qinling and the Tertiary sandstones of the Linxia basin. The change in channel steepness across this boundary due to differences in lithology is minor compared with the change across the knickpoints (Figures 5a–5c). This observation, coupled with the fact that the main stem Daxia River is markedly steeper than tributaries that are confined to the Tertiary rocks in the Linxia basin (Figure 5), suggest that the lower reaches of the system are governed largely by the upstream sediment supply [cf. *Duvall et al.*, 2004]. These results suggest a potential complication in channel profile response, in that the difference in rock strength across the boundary at the margin of the Linxia basin may have engendered a steepening of the transport gradient required to move coarse sediment during headward progression of the incisional wave. Similar observations were reported for channels in Utah [*Johnson et al.*, 2009] and were recently argued for channels into which large hillslope blocks are delivered [*Shobe et al.*, 2016]. Thus, our results highlight the possibility that the morphologic characteristics of the Daxia River suggestive of detachment-limited behavior (i.e., slope-break knickpoints) may have developed during transient incision along a channel system whose gradients are transport-limited [e.g., *Gasparini et al.*, 2007; *Yanites and Tucker*, 2010]. Although a definitive test of this hypothesis remains to be conducted, our results provide strong support for the likelihood of transport-limited conditions during transient incision [*Cowie et al.*, 2008]. If so, our results would carry important implications for the applicability of standard stream-power type inverse models to infer uplift histories at continental scales [e.g., *Roberts and White*, 2010], suggesting that conventional notions of how to relate the morphology of transient knickpoints to their behavior [e.g., *Kirby and Whipple*, 2012] may be incomplete.

6. Conclusions

Our study of the response of the Daxia River to Pleistocene base-level fall along the main stem Yellow River leads to the following conclusions. First, geomorphic analyses of topographic slope, relief, and the morphology of channel longitudinal profiles confirm that the drainage basin is in a transient state. Major knickzones separate upstream low-relief topography and gentler channel slopes from downstream steeper landscape in

the process of adjusting to the base-level fall. Second, measurements of erosion and incision rate associated with these different portions of the landscape reveal that the high-relief landscape downstream of knickpoints is eroding 3 times faster than that of the catchments above the knickpoints. Third, surveys of reach-scale channel geometry, slope, discharge, and grain size allow estimation of the basal shear stress, unit stream power, and bed load transport capacity along the main stem of the Daxia River. These results reveal a downstream increase of transport capacity, consistent with a response to increasing sediment supply. Fourth, despite differences in erosion rate and sediment supply, we find no significant narrowing of the channel across knickpoints. Our results suggest that the lower reaches of the transient system are governed largely by the upstream sediment yield. Thus, we conclude that differences in the pace and style of channel width adjustment in regions experiencing relatively low erosion rates evolve as a consequence of sediment supply and bed load transport capacity.

References

Allen, G. H., J. B. Barnes, T. M. Pavelsky, and E. Kirby (2013), Lithologic and tectonic controls on bedrock channel form at the northwest Himalayan front, *J. Geophys. Res. Earth Surf.*, *118*, 1806–1825, doi:10.1002/jgrf.20113.

Amos, C. B., and D. W. Burbank (2007), Channel width response to differential uplift, *J. Geophys. Res.*, *112*, F02010, doi:10.1029/2006JF000672.

An, Z., et al. (2015), Global monsoon dynamics and climate change, *Annu. Rev. Earth Planet. Sci.*, *43*(1), 29–77, doi:10.1146/annurev-earth-060313-054623.

Andrews, E. D. (1984), Bed material entrainment and hydraulic geometry of gravel-bed rivers in Colorado, *Geol. Soc. Am. Bull.*, *95*, 371–378.

Attal, M., G. E. Tucker, A. C. Whittaker, P. A. Cowie, and G. P. Roberts (2008), Modeling fluvial incision and transient landscape evolution: Influence of dynamic channel adjustment, *J. Geophys. Res.*, *113*, F03013, doi:10.1029/2007JF000893.

Attal, M., and J. Lavé (2006), Changes of bedload characteristics along the Marsyandi River (central Nepal): Implications for understanding hillslope sediment supply, sediment load evolution along fluvial networks, and denudation in active orogenic belts, *Geol. Soc. of Am. Spec. Pap.*, *398*, 143–171, doi:10.1130/2006.2398(09).

Attal, M., P. A. Cowie, A. C. Whittaker, D. Hobley, G. E. Tucker, and G. P. Roberts (2011), Testing fluvial erosion models using the transient response of bedrock rivers to tectonic forcing in the Apennines, Italy, *J. Geophys. Res.*, *116*, F02005, doi:10.1029/2010JF001875.

Attal, M., S. M. Mudd, M. D. Hurst, B. Weinman, K. Yoo, and M. Naylor (2015), Impact of change in erosion rate and landscape steepness on hillslope and fluvial sediments grain size in the Feather River basin (Sierra Nevada, California), *Earth Surf. Dynam.*, *3*(1), 201–222, doi:10.5194/esurf-3-201-2015.

Bellin, N., V. Vanacker, and P. W. Kubik (2014), Denudation rates and tectonic geomorphology of the Spanish Baetic Cordillera, *Earth Planet. Sci. Lett.*, *390*, 19–30, doi:10.1016/j.epsl.2013.12.045.

Berlin, M. M., and R. S. Anderson (2007), Modeling of knickpoint retreat on the Roan Plateau, western Colorado, *J. Geophys. Res.*, *112*, F03S06, doi:10.1029/2006JF000553.

Bierman, P., and E. J. Steig (1996), Estimating rates of denudation using cosmogenic isotope abundances in sediment, *Earth Surf. Processes Landforms*, *21*(2), 125–139, doi:10.1002/(SICI)1096-9837(199602)21:2<125::AID-ESP511>3.0.CO;2-8.

Bishop, P., T. B. Hoey, J. D. Jansen, and I. L. Artza (2005), Knickpoint recession rate and catchment area: The case of uplifted rivers in Eastern Scotland, *Earth Surf. Processes Landforms*, *30*(6), 767–778, doi:10.1002/esp.1191.

Burbank, D. W., J. Leland, E. Fielding, R. S. Anderson, N. Brozovic, M. R. Reid, and C. Duncan (1996), Bedrock incision, rock uplift and threshold hillslopes in the northwestern Himalayas, *Nature*, *379*(6565), 505–510, doi:10.1038/379505a0.

Bureau of Geology and Mineral Resources (BGMR) Gansu Province (1989), *Regional Geology of the Gansu Province*, pp. 1–692, Geol. House, Beijing.

Clark, M. K., K. A. Farley, D. Zheng, Z. Wang, and A. R. Duvall (2010), Early Cenozoic faulting of the northern Tibetan Plateau margin from apatite (U-Th)/He ages, *Earth Planet. Sci. Lett.*, *296*(1–2), 78–88, doi:10.1016/j.epsl.2010.04.051.

Codilean, A. T. (2006), Calculation of the cosmogenic nuclide production topographic shielding scaling factor for large areas using DEMs, *Earth Surf. Processes Landforms*, *31*(6), 785–794, doi:10.1002/esp.1336.

Cowie, P. A., A. C. Whittaker, M. Attal, G. Roberts, G. E. Tucker, and A. Ganas (2008), New constraints on sediment-flux-dependent river incision: Implications for extracting tectonic signals from river profiles, *Geology*, *36*(7), 535–538, doi:10.1130/g24681a.1.

Craddock, W., E. Kirby, and H. Zhang (2011), Late Miocene-Pliocene range growth in the interior of the northeastern Tibetan Plateau, *Lithosphere*, *3*(6), 420–438, doi:10.1130/l159.1.

Craddock, W. H., E. Kirby, N. W. Harkins, H. P. Zhang, X. H. Shi, and J. H. Liu (2010), Rapid fluvial incision along the Yellow River during headward basin integration, *Nat. Geosci.*, *3*(3), 209–213, doi:10.1038/Ngeo777.

Crosby, B. T., and K. X. Whipple (2006), Knickpoint initiation and distribution within fluvial networks: 236 waterfalls in the Waipaoa River, North Island, New Zealand, *Geomorphology*, *82*(1–2), 16–38, doi:10.1016/j.geomorph.2005.08.023.

DiBiase, R. A., and K. X. Whipple (2011), The influence of erosion thresholds and runoff variability on the relationships among topography, climate, and erosion rate, *J. Geophys. Res.*, *116*, F04036, doi:10.1029/2011JF002095.

DiBiase, R. A., K. X. Whipple, A. M. Heimsath, and W. B. Ouimet (2010), Landscape form and millennial erosion rates in the San Gabriel Mountains, CA, *Earth Planet. Sci. Lett.*, *289*(1–2), 134–144, doi:10.1016/j.epsl.2009.10.036.

Duvall, A., E. Kirby, and D. Burbank (2004), Tectonic and lithologic controls on bedrock channel profiles and processes in coastal California, *J. Geophys. Res.*, *109*, F03002, doi:10.1029/2003JF000086.

Duvall, A. R., M. K. Clark, B. A. van der Pluijm, and C. Li (2011), Direct dating of Eocene reverse faulting in northeastern Tibet using Ar-dating of fault clays and low-temperature thermochronometry, *Earth Planet Sc Lett*, *304*(3–4), 520–526, doi:10.1016/j.epsl.2011.02.028.

Emmett, W. W. (1975), The channels and waters of the Upper Salmon River area, Idaho, U.S. Geol. Surv. Prof. Pap., 870-A, 115 pp.

Fang, X., C. Garzione, R. Van der Voo, J. Li, and M. Fan (2003), Flexural subsidence by 29 Ma on the NE edge of Tibet from the magnetostratigraphy of Linxia basin, China, *Earth Planet. Sci. Lett.*, *210*(3–4), 545–560, doi:10.1016/S0012-821x(03)00142-0.

Finnegan, N. J., G. Roe, D. R. Montgomery, and B. Hallet (2005), Controls on the channel width of rivers: Implications for modeling fluvial incision of bedrock, *Geology*, *33*(3), 229–232, doi:10.1130/g21171.1.

Fisher, G. B., C. B. Amos, B. Bookhagen, D. W. Burbank, and V. Godard (2012), Channel widths, landslides, faults, and beyond: The new world order of high-spatial resolution Google Earth imagery in the study of Earth surface processes, *Geol. Soc. Am. Bull. Spec. Pap.*, *492*, 1–22, doi:10.1130/2012.2492(01).

Fisher, G. B., B. Bookhagen, and C. B. Amos (2013), Channel planform geometry and slopes from freely available high-spatial resolution imagery and DEM fusion: Implications for channel width scalings, erosion proxies, and fluvial signatures in tectonically active landscapes, *Geomorphology*, *194*, 46–56, doi:10.1016/j.geomorph.2013.04.011.

Flint, J. J. (1974), Stream gradient as a function of order, magnitude, and discharge, *Water Resour. Res.*, *10*(5), 969–973, doi:10.1029/WR010i005p00969.

Fox, M., L. Goren, D. A. May, and S. D. Willett (2014), Inversion of fluvial channels for paleorock uplift rates in Taiwan, *J. Geophys. Res. Earth Surf.*, *119*, 1853–1875, doi:10.1002/2014JF003196.

Fox, M., T. Bodin, and D. L. Shuster (2015), Abrupt changes in the rate of Andean Plateau uplift from reversible jump Markov chain Monte Carlo inversion of river profiles, *Geomorphology*, *238*, 1–14, doi:10.1016/j.geomorph.2015.02.022.

Gasparini, N. M., K. X. Whipple, and R. L. Bras (2007), Predictions of steady state and transient landscape morphology using sediment-flux-dependent river incision models, *J. Geophys. Res.*, *112*, F03S09, doi:10.1029/2006JF000567.

Glotzbach, C. (2015), Deriving rock uplift histories from data-driven inversion of river profiles, *Geology*, *43*(6), 467–470, doi:10.1130/g36702.1.

Goren, L., M. Fox, and S. D. Willett (2014), Tectonics from fluvial topography using formal linear inversion: Theory and applications to the Inyo Mountains, California, *J. Geophys. Res. Earth Surf.*, *119*, 1651–1681, doi:10.1002/2014JF003079.

Granger, D. E., J. W. Kirchner, and R. Finkel (1996), Spatially Averaged long-term erosion rates measured from in situ-produced cosmogenic nuclides in alluvial sediment, *J. Geol.*, *104*(3), 249–257, doi:10.1086/629823.

Granger, D. E., N. A. Lifton, and J. K. Willenbring (2013), A cosmic trip: 25 years of cosmogenic nuclides in geology, *Geol. Soc. Am. Bull.*, doi:10.1130/b30774.1.

Hack, J. T. (1957), Studies of longitudinal stream profiles in Virginia and Maryland, U.S. Geol. Surv. Prof. Pap., 294-B, 1-97.

Hancock, G. S., and R. S. Anderson (2002), Numerical modeling of fluvial strath-terrace formation in response to oscillating climate, *Geol. Soc. Am. Bull.*, *114*(9), 1131–1142.

Harel, M.-A., S. M. Mudd, and M. Attal (2016), Global analysis of the stream power law parameters based on worldwide 10Be denudation rates, *Geomorphology*, *268*, 184–196, doi:10.1016/j.geomorph.2016.05.035.

Harkins, N., E. Kirby, A. Heimsath, R. Robinson, and U. Reiser (2007), Transient fluvial incision in the headwaters of the Yellow River, northeastern Tibet, China, *J. Geophys. Res.*, *112*, F03S04, doi:10.1029/2006JF000570.

Heimsath, A. M., R. A. DiBiase, and K. X. Whipple (2012), Soil production limits and the transition to bedrock-dominated landscapes, *Nat. Geosci.*, *5*(3), 210–214, doi:10.1038/NGEO1380.

Hey, R. D., and C. R. Thorne (1986), Stable channels with mobile gravel beds, *J. Hydraul. Eng.*, *112*, 671–689.

Hough, B. G., C. N. Garzione, Z. Wang, R. O. Lease, D. W. Burbank, and D. Yuan (2011), Stable isotope evidence for topographic growth and basin segmentation: Implications for the evolution of the NE Tibetan Plateau, *Geol. Soc. Am. Bull.*, *123*(1–2), 168–185, doi:10.1130/B30090.1.

Howard, A. D. (1994), A detachment-limited model of drainage basin evolution, *Water Resour. Res.*, *30*(7), 2261–2285, doi:10.1029/94WR00757.

Howard, A. D. (1998), Long profile development of bedrock channels: Interaction of weathering, mass wasting, bed erosion, and sediment transport, in *Rivers Over Rock: Fluvial Processes in Bedrock Channels*, vol. 107, edited by K. Tinkler and E. E. Wohl, pp. 297–319, AGU, Washington, D. C.

Howard, A. D., W. E. Dietrich, and M. A. Seidl (1994), Modeling fluvial erosion on regional to continental scales, *J. Geophys. Res.*, *99*(B7), 13,971–13,986, doi:10.1029/94JB00744.

Hu, X., E. Kirby, B. Pan, D. E. Granger, and H. Su (2011), Cosmogenic burial ages reveal sediment reservoir dynamics along the Yellow River, China, *Geology*, *39*(9), 839–842, doi:10.1130/g32030.1.

Johnson, J. P. L., K. X. Whipple, L. S. Sklar, and T. C. Hanks (2009), Transport slopes, sediment cover, and bedrock channel incision in the Henry Mountains, Utah, *J. Geophys. Res.*, *114*, F02014, doi:10.1029/2007JF000862.

Keulegan, G. B. (1938), Laws of turbulent flow in open channels, *J. Res. Natl. Bur. Stand. U.S.*, *21*, 707–741.

Kirby, E., and N. Harkins (2013), Distributed deformation around the eastern tip of the Kunlun fault, *Int. J. Earth Sci.*, *1–14*, doi:10.1007/s00531-013-0872-x.

Kirby, E., and W. Ouimet (2011), Tectonic geomorphology along the eastern margin of Tibet: Insights into the pattern and processes of active deformation adjacent to the Sichuan basin, in *Growth and Collapse of the Tibetan Plateau*, *Geol. Soc. Lond. Spec. Publ.*, vol. 353, edited by R. Gloaguen and L. Ratschbacher, pp. 165–188.

Kirby, E., and K. Whipple (2001), Quantifying differential rock-uplift rates via stream profile analysis, *Geology*, *29*(5), 415–418, doi:10.1130/0091-7613(2001)029<0415:QDRURV>2.0.CO;2.

Kirby, E., and K. X. Whipple (2012), Expression of active tectonics in erosional landscapes, *J. Struct. Geol.*, *44*, 54–75, doi:10.1016/j.jsg.2012.07.009.

Kirby, E., K. X. Whipple, W. Q. Tang, and Z. L. Chen (2003), Distribution of active rock uplift along the eastern margin of the Tibetan Plateau: Inferences from bedrock channel longitudinal profiles, *J. Geophys. Res.*, *108*(B4), 2217, doi:10.1029/2001JB000861.

Lague, D. (2014), The stream power river incision model: Evidence, theory and beyond, *Earth Surf. Processes Landforms*, *39*(1), 38–61, doi:10.1002/esp.3462.

Lague, D., N. Hovius, and P. Davy (2005), Discharge, discharge variability, and the bedrock channel profile, *J. Geophys. Res.*, *110*, F04006, doi:10.1029/2004JF000259.

Lal, D. (1991), Cosmic ray labeling of erosion surfaces: In situ nuclide production rates and erosion models, *Earth Planet. Sci. Lett.*, *104*(2–4), 424–439, doi:10.1016/0012-821X(91)90220-C.

Lavé, J., and J. P. Avouac (2000), Active folding of fluvial terraces across the Siwaliks Hills, Himalayas of central Nepal, *J. Geophys. Res.*, *105*, 5735–5770, doi:10.1029/1999JB900292.

Lease, R. O., D. W. Burbank, G. Gehrels, Z. Wang, and D. Yuan (2007), Signatures of mountain building: Detrital zircon U/Pb ages from northeastern Tibet, *Geology*, *35*(3), 239–242, doi:10.1130/g23057a.1.

Lease, R. O., D. W. Burbank, B. Hough, Z. Wang, and D. Yuan (2012), Pulsed Miocene range growth in northeastern Tibet: Insights from Xunhua basin magnetostratigraphy and provenance, *Geol. Soc. Am. Bull.*, *124*(5–6), 657–677, doi:10.1130/b30524.1.

Leopold, L. B., and T. Maddock Jr. (1953), The hydraulic geometry of stream channels and some physiographic implications U.S. Geol. Surv. Prof. Pap. Rep. Rep. 252, 57 pp.

Li, J. (1991), The environmental effects of the uplift of the Qinghai-Xizang Plateau, *Quat. Sci. Rev.*, *10*(6), 479–483.

Li, J. J., et al. (1997), Magnetostratigraphic dating of river terraces: Rapid and intermittent incision by the Yellow River of the northeastern margin of the Tibetan Plateau during the Quaternary, *J. Geophys. Res.*, *102*(B5), 10,121–10,132, doi:10.1029/97JB00275.

Miller, S. R., P. B. Sak, E. Kirby, and P. R. Bierman (2013), Neogene rejuvenation of central Appalachian topography: Evidence for differential rock uplift from stream profiles and erosion rates, *Earth Planet. Sci. Lett.*, *369–370*, 1–12, doi:10.1016/j.epsl.2013.04.007.

Molnar, P., R. S. Anderson, G. Kier, and J. Rose (2006), Relationships among probability distributions of stream discharges in floods, climate, bed load transport, and river incision, *J. Geophys. Res.*, *111*, F02001, doi:10.1029/2005JF000310.

Montgomery, D. R., and M. T. Brandon (2002), Topographic controls on erosion rates in tectonically active mountain ranges, *Earth Planet. Sci. Lett.*, *201*(3–4), 481–489, doi:10.1016/S0012-821X(02)00725-2.

Montgomery, D. R., and K. B. Gran (2001), Downstream variations in the width of bedrock channels, *Water Resour. Res.*, *37*(6), 1841–1846, doi:10.1029/2000WR900393.

Mueller, E. R., and J. Pitlick (2005), Morphologically based model of bed load transport capacity in a headwater stream, *J. Geophys. Res.*, *110*, F02016, doi:10.1029/2003JF000117.

Mueller, E. R., and J. Pitlick (2013), Sediment supply and channel morphology in mountain river systems: 1. Relative importance of lithology, topography, and climate, *J. Geophys. Res. Earth Surf.*, *118*, 2325–2342, doi:10.1002/2013JF002843.

Mueller, E. R., J. Pitlick, and J. Nelson (2005), Variation in the reference Shields stress for bed load transport in gravel bed streams and rivers, *Water Resour. Res.*, *41*, W04006, doi:10.1029/2004WR003692.

Niemi, N. A., M. Oskin, D. W. Burbank, A. M. Heimsath, and E. J. Gabet (2005), Effects of bedrock landslides on cosmogenically determined erosion rates, *Earth Planet. Sci. Lett.*, *237*(3–4), 480–498, doi:10.1016/j.epsl.2005.07.009.

Ouimet, W. B., K. X. Whipple, and D. E. Granger (2009), Beyond threshold hillslopes: Channel adjustment to base-level fall in tectonically active mountain ranges, *Geology*, *37*(7), 579–582, doi:10.1130/G30013A.1.

Parker, G. (1979), Hydraulic geometry of active gravel rivers, *J. Hydraul. Div. Am. Soc. Civ. Eng.*, *105*, 1185–1201.

Parker, G., P. R. Wilcock, C. Paola, W. E. Dietrich, and J. Pitlick (2007), Physical basis for quasi-universal relations describing bankfull hydraulic geometry of single-thread gravel bed rivers, *J. Geophys. Res.*, *112*, F04005, doi:10.1029/2006JF000549.

Pitlick, J., and R. Cress (2002), Downstream changes in the channel geometry of a large gravel bed river, *Water Resour. Res.*, *38*(10), 1216, doi:10.1029/2001WR000898.

Pritchard, D., G. G. Roberts, N. J. White, and C. N. Richardson (2009), Uplift histories from river profiles, *Geophys. Res. Lett.*, *36*, L24301, doi:10.1029/2009GL040928.

Roberts, G. G., and N. White (2010), Estimating uplift rate histories from river profiles using African examples, *J. Geophys. Res.*, *115* B02406, doi:10.1029/2009JB006692.

Roberts, G. G., N. J. White, G. L. Martin-Brandis, and A. G. Crosby (2012), An uplift history of the Colorado Plateau and its surroundings from inverse modeling of longitudinal river profiles, *Tectonics*, *31*, TC4022, doi:10.1029/2012TC003107.

Rosenbloom, N. A., and R. S. Anderson (1994), Hillslope and channel evolution in a marine terraced landscape, Santa Cruz, California, *J. Geophys. Res.*, *99*(B7), 14,013–14,029, doi:10.1029/94JB00048.

Royden, L., and J. Taylor Perron (2013), Solutions of the stream power equation and application to the evolution of river longitudinal profiles, *J. Geophys. Res. Earth Surf.*, *118*, 497–518, doi:10.1002/jgrf.20031.

Rudge, J. F., G. G. Roberts, N. J. White, and C. N. Richardson (2015), Uplift histories of Africa and Australia from linear inverse modeling of drainage inventories, *J. Geophys. Res. Earth Surf.*, *120*, 894–914, doi:10.1002/2014JF003297.

Schildgen, T. F., D. Cosentino, B. Bookhagen, S. Niedermann, C. Yıldırım, H. Echtler, H. Wittmann, and M. R. Strecker (2012), Multi-phased uplift of the southern margin of the Central Anatolian plateau, Turkey: A record of tectonic and upper mantle processes, *Earth Planet. Sci. Lett.*, *317–318*, 85–95, doi:10.1016/j.epsl.2011.12.003.

Schmidt, K. M., and D. R. Montgomery (1995), Limits to relief, *Science*, *270*(5236), 617–620, doi:10.1126/science.270.5236.617.

Schoenbohm, L. M., K. X. Whipple, B. C. Burchfiel, and L. Chen (2004), Geomorphic constraints on surface uplift, exhumation, and plateau growth in the Red River region, Yunnan Province, China, *Geol. Soc. Am. Bull.*, *116*(7–8), 895–909, doi:10.1130/b25364.1.

Shobe, C. M., G. E. Tucker, and R. S. Anderson (2016), Hillslope-derived blocks retard river incision, *Geophys. Res. Lett.*, *43*, 5070–5078, doi:10.1002/2016GL069262.

Sklar, L. S., and W. E. Dietrich (2004), A mechanistic model for river incision into bedrock by saltating bed load, *Water Resour. Res.*, *40*(6), W06301, doi:10.1029/2003WR002496.

Snyder, N. P., K. X. Whipple, G. E. Tucker, and D. J. Merritts (2000), Landscape response to tectonic forcing: Digital elevation model analysis of stream profiles in the Mendocino triple junction region, Northern California, *Geol. Soc. Am. Bull.*, *112*(8), 1250–1263, doi:10.1130/0016-7606 (2000)112<1250:LRTTFD>2.0.CO;2.

Snyder, N. P., K. X. Whipple, G. E. Tucker, and D. J. Merritts (2003a), Channel response to tectonic forcing: Field analysis of stream morphology and hydrology in the Mendocino triple junction region, northern California, *Geomorphology*, *53*(1–2), 97–127, doi:10.1016/S0169-555X(02)00349-5.

Snyder, N. P., K. X. Whipple, G. E. Tucker, and D. J. Merritts (2003b), Importance of a stochastic distribution of floods and erosion thresholds in the bedrock river incision problem, *J. Geophys. Res.*, *108*(2), 2117, doi:10.1029/2001JB001655.

Stark, C. P. (2006), A self-regulating model of bedrock river channel geometry, *Geophys. Res. Lett.*, *33*, L04402, doi:10.1029/2005GL023193.

Stephenson, S. N., G. G. Roberts, M. J. Hoggard, and A. C. Whittaker (2014), A Cenozoic uplift history of Mexico and its surroundings from longitudinal river profiles, *Geochem. Geophys. Geosyst.*, *15*, 4734–4758, doi:10.1002/2014GC005425.

Stone, J. O. (2000), Air pressure and cosmogenic isotope production, *J. Geophys. Res.*, *105*(B10), 23,753–23,759, doi:10.1029/2000JB900181.

Tomkin, J. H., M. T. Brandon, F. J. Pazzaglia, J. R. Barbour, and S. D. Willett (2003), Quantitative testing of bedrock incision models for the Clearwater River, NW Washington State, *J. Geophys. Res.*, *108*(B6), 2308, doi:10.1029/2001JB000862.

Tucker, G. E. (2004), Drainage basin sensitivity to tectonic and climatic forcing: Implications of a stochastic model for the role of entrainment and erosion thresholds, *Earth Surf. Processes Landforms*, *29*(2), 185–205, doi:10.1002/esp.1020.

Tucker, G. E., and R. L. Bras (2000), A stochastic approach to modeling the role of rainfall variability in drainage basin evolution, *Water Resour. Res.*, *36*(7), 1953–1964, doi:10.1029/2000WR900065.

Tucker, G. E., and K. X. Whipple (2002), Topographic outcomes predicted by stream erosion models: Sensitivity analysis and intermodel comparison, *J. Geophys. Res.*, *107*(B9), 2179, doi:10.1029/2001JB000162.

Turowski, J. M., D. Lague, and N. Hovius (2007), Cover effect in bedrock abrasion: A new derivation and its implications for the modeling of bedrock channel morphology, *J. Geophys. Res.*, *112*, F04006, doi:10.1029/2006JF000697.

Valla, P. G., P. A. van der Beek, and D. Lague (2010), Fluvial incision into bedrock: Insights from morphometric analysis and numerical modeling of gorges incising glacial hanging valleys (Western Alps, France), *J. Geophys. Res.*, *115*, F02010, doi:10.1029/2008JF001079.

van der Beek, P., and P. Bishop (2003), Cenozoic river profile development in the Upper Lachlan catchment (SE Australia) as a test of quantitative fluvial incision models, *J. Geophys. Res.*, *108*(B6), 2309, doi:10.1029/2002JB002125.

Vermeesch, P. (2007), CosmoCalc: An Excel add-in for cosmogenic nuclide calculations, *Geochem. Geophys. Geosyst.*, *8*, Q08003, doi:10.1029/2006GC001530.

Wegmann, K. W., and F. J. Pazzaglia (2002), Holocene strath terraces, climate change, and active tectonics: The Clearwater River basin, Olympic Peninsula, Washington State, *Geol. Soc. Am. Bull.*, *114*(6), 731–744, doi:10.1130/0016-7606(2002)114<0731:HSTCCA>2.0.CO;2.

Whipple, K. X. (2004), Bedrock rivers and the geomorphology of active orogens, *Annu. Rev. Earth Planet. Sci.*, *32*, 151–185, doi:10.1146/annurev.earth.32.101802.120356.

Whipple, K. X., and G. E. Tucker (1999), Dynamics of the stream-power river incision model: Implications for height limits of mountain ranges, landscape response timescales, and research needs, *J. Geophys. Res.*, *104*(B8), 17,661–17,674, doi:10.1029/1999JB900120.

Whipple, K. X., and G. E. Tucker (2002), Implications of sediment-flux-dependent river incision models for landscape evolution, *J. Geophys. Res.*, *107*(B2), 2039, doi:10.1029/2000JB000044.

Whipple, K. X., E. Kirby, and S. H. Brocklehurst (1999), Geomorphic limits to climate-induced increases in topographic relief, *Nature*, *401*(6748), 39–43, doi:10.1038/43375.

Whipple, K. X., G. S. Hancock, and R. S. Anderson (2000), River incision into bedrock: Mechanics and relative efficacy of plucking, abrasion, and cavitation, *Geol. Soc. Am. Bull.*, *112*(3), 490–503, doi:10.1130/0016-7606(2000)112<490:RIIBMA>2.0.CO;2.

Whitbread, K., J. Jansen, P. Bishop, and M. Attal (2015), Substrate, sediment, and slope controls on bedrock channel geometry in postglacial streams, *J. Geophys. Res. Earth Surf.*, *120*, 779–798, doi:10.1002/2014JF003295.

Whittaker, A. C. (2012), How do landscapes record tectonics and climate?, *Lithosphere*, *4*(2), 160–164, doi:10.1130/rf.l003.1.

Whittaker, A. C., P. A. Cowie, M. Attal, G. E. Tucker, and G. P. Roberts (2007a), Bedrock channel adjustment to tectonic forcing: Implications for predicting river incision rates, *Geology*, *35*(2), 103–106, doi:10.1130/g23106a.1.

Whittaker, A. C., P. A. Cowie, M. Attal, G. E. Tucker, and G. P. Roberts (2007b), Contrasting transient and steady-state rivers crossing active normal faults: New field observations from the Central Apennines, Italy, *Basin Res.*, *19*(4), 529–556, doi:10.1111/j.1365-2117.2007.00337.x.

Whittaker, A. C., M. Attal, P. A. Cowie, G. E. Tucker, and G. Roberts (2008), Decoding temporal and spatial patterns of fault uplift using transient river long profiles, *Geomorphology*, *100*(3–4), 506–526, doi:10.1016/j.geomorph.2008.01.018.

Wilson, J. W. P., G. G. Roberts, M. J. Hoggard, and N. J. White (2014), Cenozoic epeirogeny of the Arabian Peninsula from drainage modeling, *Geochem. Geophys. Geosyst.*, *15*, 3723–3761, doi:10.1002/2014GC005283.

Wobus, C., K. X. Whipple, E. Kirby, N. Snyder, J. Johnson, K. Spyropolou, B. Crosby, and D. Sheehan (2006b), Tectonics from topography: Procedures, promise, and pitfalls, *Geol. Soc. Am. Bull. Spec. Pap.*, *398*, 55–74, doi:10.1130/2006.2398(04).

Wobus, C. W., G. E. Tucker, and R. S. Anderson (2006a), Self-formed bedrock channels, *Geophys. Res. Lett.*, *33*, L18408, doi:10.1029/2006GL027182.

Wohl, E., and G. C. L. David (2008), Consistency of scaling relations among bedrock and alluvial channels, *J. Geophys. Res.*, *113*, F04013, doi:10.1029/2008JF000989.

Wolman, M. G. (1954), A method of sampling coarse river-bed material, *Trans. Am. Geophys.Union*, *35*, 951–956.

Yanites, B. J., and G. E. Tucker (2010), Controls and limits on bedrock channel geometry, *J. Geophys. Res.*, *115*, F04019, doi:10.1029/2009JF001601.

Yanites, B. J., G. E. Tucker, and R. S. Anderson (2009), Numerical and analytical models of cosmogenic radionuclide dynamics in landslide-dominated drainage basins, *J. Geophys. Res.*, *114*, F01007, doi:10.1029/2008JF001088.

Yanites, B. J., G. E. Tucker, K. J. Mueller, Y.-G. Chen, T. Wilcox, S.-Y. Huang, and K.-W. Shi (2010), Incision and channel morphology across active structures along the Peikang River, central Taiwan: Implications for the importance of channel width, *Geol. Soc. Am. Bull.*, *122*(7–8), 1192–1208.

Yuan, D. Y., J. D. Champagnac, W. P. Ge, P. Molnar, P. Z. Zhang, W. J. Zheng, H. P. Zhang, and X. W. Liu (2011), Late Quaternary right-lateral slip rates of faults adjacent to the lake Qinghai, northeastern margin of the Tibetan Plateau, *Geol. Soc. Am. Bull.*, *123*(9–10), 2016–2030, doi:10.1130/b30315.1.

Yuan, D.-Y., et al. (2013), The growth of northeastern Tibet and its relevance to large-scale continental geodynamics: A review of recent studies, *Tectonics*, *32*, 1358–1370, doi:10.1002/tect.20081.

Zhang, H., P. Zhang, J.-D. Champagnac, P. Molnar, R. S. Anderson, E. Kirby, W. H. Craddock, and S. Liu (2014), Pleistocene drainage reorganization driven by the isostatic response to deep incision into the northeastern Tibetan Plateau, *Geology*, *42*(4), 303–306, doi:10.1130/g35115.1.

Zhang, H.-P., W. H. Craddock, R. O. Lease, W.-t. Wang, D.-Y. Yuan, P.-Z. Zhang, P. Molnar, D.-W. Zheng, and W.-J. Zheng (2012), Magnetostratigraphy of the Neogene Chaka basin and its implications for mountain building processes in the north-eastern Tibetan Plateau, *Basin Res.*, *24*(1), 31–50, doi:10.1111/j.1365-2117.2011.00512.x.